Final Report

Covering the Period 15 April 1972 to 30 June 1975

29 August 1975

STUDIES OF E-BEAM PUMPED MOLECULAR LASERS

By: R. A. GUTCHECK, R. M. HILL, D. L. HUESTIS, D. C. LORENTS, and M. V. McCUSKER

SRI No. MP 75-43

Prepared for:

ADVANCED RESEARCH PROJECTS AGENCY
WASHINGTON, D.C. 20301

DIRECTOR OF PHYSICS PROGRAMS, PHYSICAL SCIENCES DIVISION
OFFICE OF NAVAL RESEARCH
DEPARTMENT OF THE NAVY
800 NORTH QUINCY STREET
ARLINGTON, VIRGINIA 22217

Sponsored by:

ADVANCED RESEARCH PROJECTS AGENCY
ARPA Order No. 1807
Contract N00014-72-C-0478
Contract Amount $494,217

Program Code No. 5E20
(15 April 1972-30 June 1975)
SRI Project PYU-1925

STANFORD RESEARCH INSTITUTE
Menlo Park, California 94025 · U.S.A.

SECURITY CLASSIFICATION OF THIS PAGE (When Data Entered)

REPORT DOCUMENTATION PAGE

READ INSTRUCTIONS BEFORE COMPLETING FORM

1. REPORT NUMBER

2. GOVT ACCESSION NO. AD-A159 696

3. RECIPIENT'S CATALOG NUMBER

4. TITLE (and Subtitle)
STUDIES OF E-BEAM PUMPED MOLECULAR LASERS

5. TYPE OF REPORT & PERIOD COVERED
Final Report - 15 April 1972 to 30 June 1975

6. PERFORMING ORG. REPORT NUMBER
SRI MP 75-43

7. AUTHOR(s)
R. A. Gutcheck, R. M. Hill, D. L. Huestis, D. C. Lorents, and M. V. McCusker

8. CONTRACT OR GRANT NUMBER(s)
N00014-72-C-0478

9. PERFORMING ORGANIZATION NAME AND ADDRESS
Stanford Research Institute
333 Ravenswood Avenue
Menlo Park, CA 94025

10. PROGRAM ELEMENT, PROJECT, TASK AREA & WORK UNIT NUMBERS
Program Code No. 5E20

11. CONTROLLING OFFICE NAME AND ADDRESS
Advanced Research Projects Agency
1400 Wilson Boulevard
Arlington, VA 22209

12. REPORT DATE
29 August 1975

13. NUMBER OF PAGES
72

14. MONITORING AGENCY NAME & ADDRESS (if different from Controlling Office)
Office of Naval Research
800 N. Quincy Street
Arlington, VA 22217

15. SECURITY CLASS. (of this report)
Unclassified

15a. DECLASSIFICATION/DOWNGRADING SCHEDULE

16. DISTRIBUTION STATEMENT (of this Report)
Unlimited distribution

This document has been approved for public release and sale; its distribution is unlimited.

17. DISTRIBUTION STATEMENT (of the abstract entered in Block 20, if different from Report)

18. SUPPLEMENTARY NOTES
(cont'd p B)

19. KEY WORDS (Continue on reverse side if necessary and identify by block number)
Electron Beam; Energy Transfer; Molecular Laser; Rare Gas Dimers; Xenon; Mercury; Ultraviolet Lamp; and Ultraviolet Spectroscopy.

20. ABSTRACT (Continue on reverse side if necessary and identify by block number)
This report contains a brief review of the results obtained in this program which was three year program, which has been designed to examine prospective high power, high efficiency laser media. These studies have included measurements of the optical emissions and temporal behavior of excited states in dense vapors and gas mixtures excited by intense, pulsed electron beams. In addition, detailed models of the excitation, relaxation, and decay kinetics of excited states have been realized for the case of Ar-N_2, Xe-O_2, and Xe-Hg mixtures. (cont.)

DD FORM 1 JAN 73 1473 EDITION OF 1 NOV 65 IS OBSOLETE

SECURITY CLASSIFICATION OF THIS PAGE (When Data Entered)

20. Abstract

In this report, we also examine in detail the spectral and temporal properties of emissions coming from mixtures of Xe and Hg, a prototype of rare gas-metal atom excimer systems, and determine some relevant rate constants. Significant fluorescent yields from weakly bound Xe-Hg excimer radiations suggest the possibility of a good UV pump source (near 270 nm) which could be used for photolytic production of $I(^2P_{\frac{1}{2}})$. A model of the energy pathways has been constructed, and it is concluded that laser action may be possible on the bands arising from the Hg 7^3S levels.

CONTENTS

ILLUSTRATIONS

TABLES

I SUMMARY

The purpose of this program is to develop an understanding of the molecular kinetics pertinent to new high efficiency, high power electronic transition lasers. We are studying high pressure gases that are initially excited by intense bursts of electrons. This initial pumping energy, which is primarily deposited by creating atomic ions, rapidly collects in the lowest molecular excited state with an overall efficiency for the rare gases near 50%.

Rare gas dimers for which the ground level is repulsive, in particular Xe_2, Kr_2, and Ar_2, have already demonstrated laser action but with disappointing efficiencies. This problem, coupled with the relatively high gain and with vacuum ultraviolet wavelengths, has led us to consider ways of transferring the energy deposited in the rare gas to other radiators to improve total efficiency, and shift the wavelength to the near ultraviolet or visible.

This report contains a brief review of all the results obtained in this program and a detailed discussion of the work done recently on the Xe-Hg excimer system. The review section outlines the results of our kinetic modelling studies and predictions for the following potential laser media: Hg (Hg_2^* is the radiator), Ar-N_2 [$N_2(C)$, $N_2(B)$, and $N_2(A)$], Xe-O_2 (XeO^* excimer) and Ar-I_2 (I_2^* at 3420 Å).

The Xe-Hg study is a prototype of the rare gas, metal atom excimer system. The most important conclusions reached for this mixture are, in summary:

1. Energy is transferred efficiently from Xe excited states to the principal excited states of Hg: 7^3S and 6^3P.
2. Radiations are observed from weakly bound Xe-Hg excimers with significant fluorescent yields.

3. Laser action seems possible on the bands arising from the Hg 7^3S level. The relative gain of the bands arising from the Hg $6^3P_{1,2}$ levels is less by a factor of 100, suggesting that laser action on these transitions may be difficult. The fluorescence yield for one of these bands (2700 Å) is sufficiently high (> 20%) to make it an attractive pump source.

4. A model of the energy pathways has been constructed which includes

   (a) collisional equilibrium among the excited states of xenon, between the Hg 7^3S level and the xenon excited states, and between the Xe-Hg 6^3P excimer levels and the Hg 6^3P_J atomic levels,

   (b) loss of Xe-Hg 6^3P levels only by radiation and formation of Hg_2 excimers.

We made calibrated measurements of the photon flux from each of the relevant radiation levels (Xe_2^* and $Xe\text{-}Hg^*$), enabling us to determine fluorescent yields and efficiencies. In addition, the temporal decay of these bands following pulsed e-beam excitation was used to determine several of the relevant rate constants.

II OVERVIEW OF THE PROGRAM

The research effort described here occurred during the period from May 1972 to July 1975. The objective of this program was to make experimental and theoretical studies of high pressure gases and gas mixtures and to determine the feasibility of laser action in such systems. This effort was particularly motivated by the hope of understanding media that would lead to the development of high-efficiency, high-power electronic transition lasers that would be useful to the DoD mission.

The great variety of the DoD applications suggests that several new lasers with different properties are needed in addition to the well known ir lasers now available. The general aim of our research effort was to develop, where possible, a systematic approach to the understanding of new laser media. With this knowledge, laser systems with specific properties necessary for a particular application might be tailored in the laboratory, tested, and scaled to large size with maximum speed and a minimum of wasted design development.

As our program developed, we sought methods to convert the energy available in the rare gas excited states created by e-beam pumping to other species that may demonstrate laser action in the visible or near uv range. Our approach was to collisionally transfer electronic excitation of the rare gas directly to electronic states of other radiating systems (atoms or molecules) to achieve the population inversions necessary for lasing. We have successfully applied this technique of energy transfer to produce media that are efficient and scalable lasers, and have developed kinetic models that accurately predict the operating characteristics of these systems and suggest new ones to survey. This method of pumping offers the freedom of choice of the radiator to select desired characteristics, such as wavelength, transition probability, and efficiency.

For high-energy, high-power lasers two modes of operation are possible. If a fast radiating transition is used, the laser energy can be removed as quickly as the laser medium is pumped, and most of the energy storage will be maintained in the power supply. However, if a metastable upper level is used, it can accumulate and store energy for a relatively long period and release it in short high-energy pulses. Both alternatives are useful, but the present DoD needs require quasi-cw operation. To facilitate the construction of high-power cw lasers, these states should have short radiative lifetimes (10^{-8} to 10^{-5} sec), be strongly resistant to quenching, and, of course, the lower level should be unpopulated and strongly quenched by either radiation or collision. To maintain high efficiency, the transfer from the noble gas to the acceptor must be quite specific.

Considering the large number of candidate molecules and the lack of understanding of energy transfer processes among excited electronic states, the choice of acceptor molecules that will lead to useful lasers cannot be determined on an a priori basis. A crucial portion of this program has involved a spectroscopic survey of emissions produced in e-beam-excited gas mixtures. While the atmospheric gases have well known kinetics and spectroscopy, this is not generally true for the excited levels of the heavier di- and tri-atomics, particularly in the presence of e-beam pumped noble gases. A significant possibility exists of creating excited molecules containing a noble gas atom, for example, XeO^* or XeI^*. Upon discovering suitably intense radiators, our course has been to study the time dependence of the radiation as a function of density and the fluorescence yield to determine whether a significant possibility of lasing actually exists. Following confirmation, a detailed experimental study is carried out to obtain rate constants and develop a detailed kinetic model of e-beam pumped laser systems of the best candidates.

While we have restricted our studies to a rather specific excitation mechanism, the scope of this program has been broad. The energy available from the various noble gas molecules ranges from 7.2 eV for Xe_2^* to nearly

20 eV for He_2^*, and the large choice of acceptor species provides many promising laser candidates.

The initial studies in this program were made on the pure mercury system. In parallel, a study of the kinetics of pure rare gases was carried out, supported directly by ONR. As work progressed, significant efforts were devoted to gas mixtures, such as argon/nitrogen and xenon/oxygen. Most recently we have focused our attention on mixed gas-metal systems, such as the xenon/mercury reported in detail in this final report and also noble gas halogen mixtures, such as argon/iodine.

The results of these studies have been documented in a series of technical reports. Here we briefly recapitulate the salient features of each of those reports.

Report No. 1 (November 1972) described the studies of the Hg_2 excimer. Mercury and other van der Waals molecules were considered to be promising candidates for laser action because the molecular radiation arises from a transition between a stable excited level and a repulsive ground state that remains essentially unpopulated. Thus, a population inversion should be readily achieved. Relatively high efficiencies of conversion of input energy to laser energy were also expected for van der Waals systems. On the other hand, since the molecular radiation is a continuum with a bandwidth on the order of hundreds of Å, the optical gain is much smaller for a given population inversion than for comparable bound-bound atomic transitions having linewidths that are several orders of magnitude narrower.

We directed our attention to the study of the Hg continuum radiation near 4800 Å, because of the potential applications of lasers at this wavelength. A theoretical model of the processes taking place in the gas was developed.

Excitation of Hg vapor was provided by a 10-joule, 3 nsec pulse of 500 keV electrons from a Febetron 706. Experiments included photographic and time-resolved emission spectroscopy of both atomic and molecular

radiation. Our observations were summarized as follows: For pressures above 1 atm, the atomic ions and highly excited atoms are rapidly channeled down to atomic levels with energies less than the molecular ionization level. All excited atomic state populations disappear in times ranging from a few μsec at 1 atm to approximately 100 nsec at 10 atm. The primary molecular mercury continuum band extends from 3900 to 4900 Å with the peak intensity near 4570 Å. Secondary continua occur in the 5100-6000 Å and 3000-3600 Å regions.

Analysis of the molecular radiation at 4570 Å indicated that the transition had a radiative lifetime of approximately 20 μsec, but had a nonexponential behavior due to quenching collisions between two excited molecules. The relatively long radiative lifetime and wide bandwidth of the Hg_2 continuum radiation led to the prediction of a very small optical gain of 5×10^{-20} per cm per excited molecule/cm^3 or 0.01/cm for 2×10^{17} molecules/cm^3.

The next technical report (July 1973) indicated that despite the attractive energy storage capabilities of Hg_2, this molecular system had significant shortcomings. We found that the absorption cross section of the dimer is greater than the stimulated emission cross section, resulting in net absorption throughout the 4570 Å continuum band. Laser action on this band in mercury was judged to be unlikely.

Mercury remains an attractive medium for energy storage, but practical use of this storage would be greatly helped by a better understanding of the molecular states of Hg_2 and the possible states of Hg_3. We included in the report a re-appraisal of the Hg_2 states intended to stimulate further thinking about this subject.

In the meantime, pure rare gas dimers, in particular Xe_2 and Kr_2, had already demonstrated laser action in other laboratories, but with disappointing efficiencies. This low efficiency, coupled with the relatively high gain (implying low energy storage capacity) as well as

inconveniently short vacuum ultraviolet wavelengths, led us to consider ways of transferring the energy deposited in the rare gas to other gas molecules. This effort was made to find ways to improve total efficiency, shift the wavelength to the ultraviolet or visible, and to improve the energy storage capacity. The second technical report also contained our initial results on the mixture Ar + N_2. We observed radiation from the nitrogen C and B excited triplet states and used small additions of NO gas as a monitor of the metastable $N_2(A)$ state population. Our preliminary conclusions as reported were essentially favorable.

This system was then investigated in considerable detail and was discussed in Technical Report No. 3 (July 1974).

In summary, the three triplet excited states of N_2[$N_2(C)$, $N_2(B)$, and $N_2(A)$], the sources of second positive, first positive, and Vegard-Kaplan radiations, as well as NO(A), source of the γ bands, are all possible laser candidates with potential efficiencies between 1 and 10%. In addition, kinetic modeling, coupled with experiments to determine excited state populations and reaction rate coefficients, led to a detailed kinetic model that could be used to reliably predict laser performance.

Measurements were made of the density of the excited N_2 states and their temporal behavior following the excitation of the argon. $N_2(C)$ and $N_2(B)$ were monitored by their radiation, but the $N_2(A)$ density was determined by adding NO as a tracer. These measurements allowed us to determine a number of reaction rate coefficients, which could be combined with others obtained from the literature to construct a kinetic model. The kinetic model computer program included some 32 reactions and had a self-determining time step, which reduced the computing time significantly. The results of the model and of the experiments agreed over a wide range of experimental parameters.

The model was used to find optimum conditions of each potential laser state and to predict the expected efficiencies. For the $N_2(C)$ state, the

predictions of laser action, efficiency, and operating parameters have been confirmed by subsequent work at other laboratories, and the model has been used in other laboratories to aid in the scaling and understanding of the Ar + N_2 laser.

Following the development of this complete model, we turned our attention to mixtures of xenon and oxygen. This work was described in Technical Report No. 4 (January 1975).

Measurements were made of the density of the Xe_2^* and XeO excimers and their temporal behavior by observing their radiations following excitation of the xenon. Estimates of the extent of O_2 dissociation were obtained from absorption measurements of the ozone produced by the recombination of the oxygen atoms. Again a preliminary kinetic model was constructed using a number of reaction rate coefficients determined by our measurements combined with others obtained from the literature. The agreement between this model and our experimental observations supports our concept of the important energy pathways and allowed the prediction of possible laser efficiencies.

The report indicated that the weakly bound excimer XeO($2^1\Sigma^+$), which is formed from Xe + O(^{1}S), is an excellent laser candidate with possible efficiencies of 6% and 11% in the green (5376 Å) and uv (3080 Å) bands, respectively. From our kinetic studies, we concluded that the production of XeO proceeds through two energy transfer steps: first, dissociation of O_2, and second, excitation of O(^{3}P) to O(^{1}S). In that report we also presented recent results of our survey program to discover other candidates for laser systems. As was indicated there, considerably more effort is necessary before the list of promising systems can be completed.

During the last period, as the result of this important survey program we discovered strong emissions near 3400 Å in argon/iodine mixtures. We subsequently measured the fluorescence yield of this molecular iodine band to be

70 ± 25%, indicating a total energy efficiency of 13 ± 4%. This work was recently discussed in Technical Report No. 5 (July 1975) and will soon be published. Since the potential curves of the iodine molecular state responsible for this emission are offset with respect to internuclear separation, we anticipated that this medium would have good prospect as a laser candidate.

We communicated these results to other laboratories; this system was subsequently found to lase in these laboratories. Continued work on this promising system has been hindered by the interruption of contract support; however, we are optimistic that proper efforts will be made to understand this mixture as well as other noble gas/halogen mixtures.

Finally, we studied in some detail the mixed gas/metal system of xenon-mercury. Our experimental results, as well as a preliminary kinetic picture, are described in this final report. We have found that one set of transitions looks promising for laser action in the visible, while another in the uv offers an efficient pump source for the iodine infrared laser.

III TECHNICAL REPORT: The Xe-Hg System

A. Introduction

The energy transfer pumping of additives contained in e-beam excited high density rare gases is a general technique for producing inversions on electronic transitions in many atomic and molecular species. It has been demonstrated that for Ar + N_2 mixtures, energy transfer pumping of the second positive system results in lasing action on the 0-1 transition (λ3576 Å)[SeH74,ABO74,NMB73,BDD74]. A previous report [HGH74] discussed the kinetics of this gas mixture in detail and gave predictions of gain and other parameters.

Our most recent report [HGH75] discussed a second system, that of XeO, which also has been shown to lase on the excimer bands related to the $O(^1S)$-$O(^1D)$ 5577 Å transition. Here the energy of the rare gas is transferred to the oxygen in a more complicated two-step process which results in the formation of a large $O(^1S)$ and XeO^* population.

Another important class of additives that can be pumped by this method is metals, all of which have electronic states lying below those of the heaviest rare gases. Because of its high vapor pressure, Hg is one of the easiest metals to study. Since we will be looking at other metal-rare gas mixtures, the Xe + Hg system can be considered representative of the other mixed excimer systems.

It was initially hoped that inversion of the 7^3S-6^3P system and of the $XeHg^*$ excimer would lead to good laser candidates. This study has revealed that these "systems" can be inverted to produce photons with significant fluorescent yields. The 7^3S transitions are potential laser candidates, and one of the excimer bands (2700 Å) may be a useful uv pump.

We discuss the experimental method, followed by a presentation of the observed results. These observations will then be analyzed in terms of the actual kinetic processes which they imply. We will then try to draw some conclusions regarding Xe-Hg as a laser and as a laser pump candidate.

B. Experiments

In this section we discuss the technique for exciting the gas mixture and for observing the subsequent emissions quantitatively. The major part of the experimental system is similar to that described in our previous reports and is schematically illustrated in Figure 1. Optical emissions, resulting from the pulsed electron excitation of the Xe-Hg mixture, are viewed by a 1/2 meter monochromator-spectrograph (McPherson Model 216.5). A Febetron 706 (Hewlett-Packard) provides a 2 to 3 nanosecond, 6000 ampere pulse of 600 keV electrons that enters a high pressure stainless steel chamber through a 1 mil Inconel foil. The cell has windows made of sapphire and is designed to operate with sample gas pressures between 500 and 5000 torr.

The Excitation Cell

This experimental cell, which is different from the one used in the XeO and Ar + N_2 studies, could be heated to temperatures between 50° and 350°C. A reservoir of Hg is continually exposed and connected to the cell, and the whole assembly is heated with cartridge heaters inserted into the metal cell and reservoir. To maintain uniformity of temperature, the cell is surrounded by maronite insulation. The temperature is monitored by thermocouples spot welded at various sites on the cell and reservoir, and all parts of the chamber are kept at approximately ($\pm$ 5°C) the same temperature for a given set of data. The lowest measured temperature is assumed to determine the Hg vapor pressure (which varied between 0.002 and 500 torr), and it is this value of Hg pressure that is used in the following sections.

The following procedure is used in the gas mixture preparation: research grade xenon is admitted to the cell when it is at room temperature,

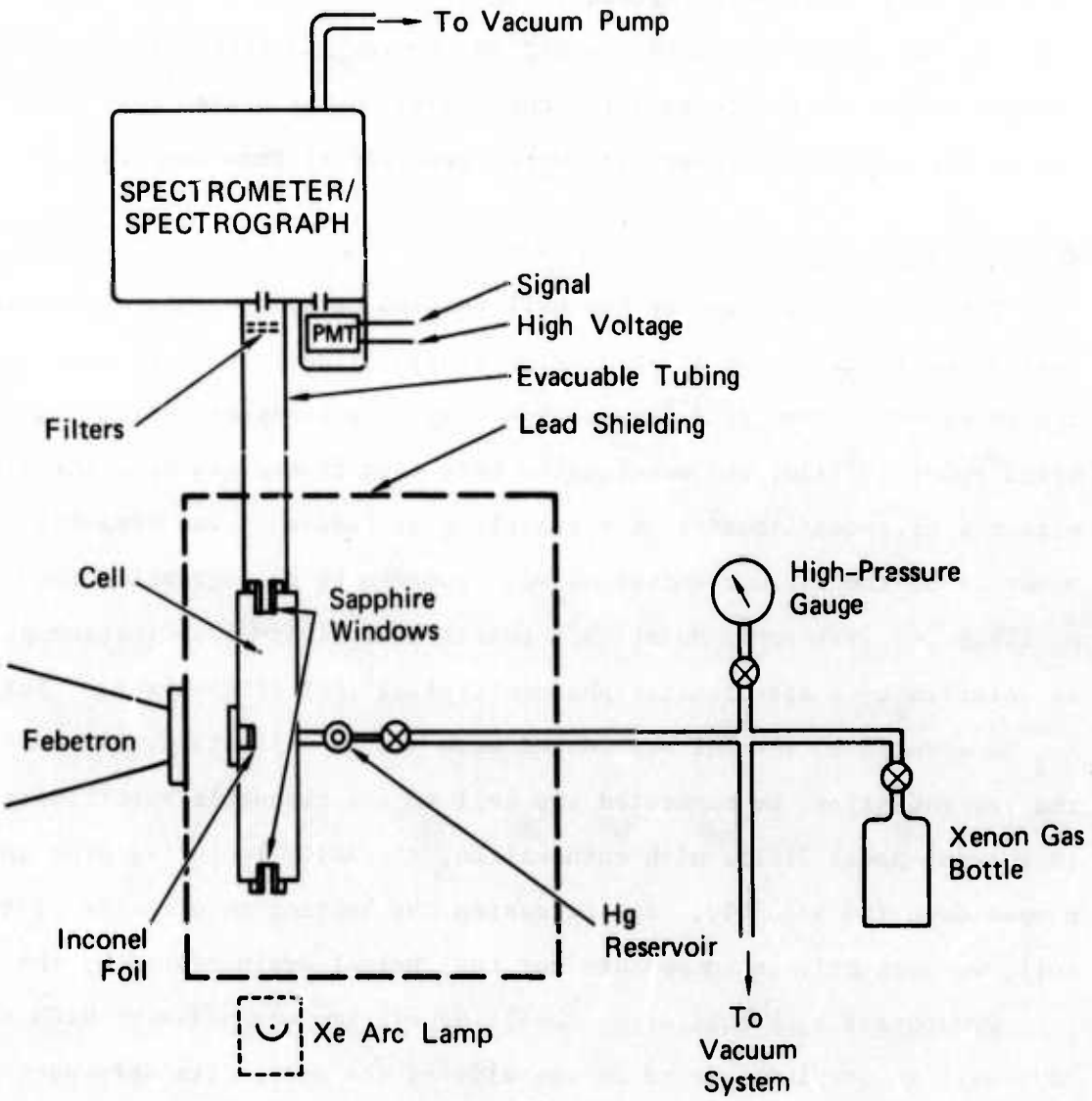

FIGURE 1 SCHEMATIC DIAGRAM OF THE EXPERIMENTAL APPARATUS

the cell is valved off, and then the temperature is raised. For each change of temperature and of xenon pressure the cell is heated for 15 hours to ensure that the Hg vapor and Xe are well mixed. A fresh batch of Xe is thus used for each pressure/temperature combination. We found that once the cell walls were exposed to Hg at a given temperature, data taken later at any lower temperature would not be reproducible. To clean the chamber walls, we had to pump for three days on the heated cell (400°C) and on the exposed Hg reservoir, which remained at room temperature.

Photon Observations

The sapphire windows on the cell enabled us to view the excitation region and to carry out an absorption study. Time-integrated spectra of the emissions (above 2100 Å) were taken by a spectrograph using high speed Polaroid film, and wavelengths were then determined with the aid of either a microdensitometer or a traveling microscope. The temporal behavior of the various emissions was recorded by photographing the oscilloscope (Tektronix Model 485) traces of individual excitation pulses as detected by a spectrometer/photomultiplier (RCA 1P28) system. For the Xe_2^* observations, the PMT was coated with sodium salicylate. To observe the vuv radiation, we connected the cell to the evacuable spectrometer (McPherson Model 216.5) with thin-walled, thermally isolating pipe and pumped down the assembly. By increasing the heating to one side of the cell, we were able to compensate for the thermal drain caused by the tubing.

Ground state absorption by the Xe-Hg mixture was measured with a 1000-watt Xe arc lamp placed on one side of the cell. Its defocused output passed through an attenuator and 2537 Å wide band (150 Å) filter. The interference filter eliminated the scattering of the more intense, longer wavelength output of the lamp. The transmitted signal through the spectrograph was recorded on film, and any absorption that occurred was measured. Uniform exposure times were taken for various cell temperatures.

For our time decay studies, we observed (a) several Hg atomic transitions in the 2967 to 5800 Å region, (b) narrow emissions at 4059, 4360, and 5461 Å [from Xe-Hg(7^3S)], and (c) wider band emissions at 2700 Å [from Xe-Hg($^3P_1$)], 2100 Å, and 1720 Å (from Xe_2^* excimer).

In computing the fluorescence yields for the various emissions, it was necessary to find the spectral response of the optical system from 1700 Å to 5400 Å. We used the same procedure given in our XeO report [HGH75], which combines the molecular branching ratio method [MuZ71] with measurements made with a standard irradiance quartz-halogen lamp [SSJ63]. For the branching ratio method, we used both the NOγ and CO 4+ bands. We do not feel the calibration at this time can give absolute values to better than a factor of 2.

C. Results

Some of the possible levels of excitation which metastable Xe^* and Xe_2^* can achieve in Hg through energy transfer are shown in Figure 2. Also, some relevant atomic Hg emissions are illustrated. The actual energy range into which the Xe_2^* excimer can transfer is between 6.8 and 7.7 eV, with the peak occurring at 7.3 eV, whereas the Xe^* metastable levels lie at 8.3 and 9.45 eV. Hence, the 7^3S level of Hg at 7.75 eV will be excited almost entirely by the atomic Xe metastables. The higher Hg level will be populated via energy transfer by either the upper metastable state or by more energetically excited Xe levels. Thus, the time scales on which the upper levels are populated should be much faster than those of the lower 6^3P levels, since the latter will reflect the buildup of the Xe_2 excimer level population and radiative cascading.

We see several types of spectra resulting from the e-beam excitation, including atomic, perturbed atomic, and excimer emissions. The characteristics of these emissions are dependent on both the total Xe pressure and the Hg partial pressure. The atomic lines are the normal Hg line emissions from upper levels (e.g., $6^3D_{1,2,3}$, 6^1D_1) of the atom, such as 5770 Å, 3650 Å, 3131 Å, 3125 Å, and 2967 Å. Under all conditions these lines are observed for only a few nanoseconds, suggesting that the upper levels are excited by energy transfer from highly excited xenon atomic levels or direct e-beam excitation. The general shape of the remaining features is shown in Figure 3, in which the flux has not been corrected for the relative spectral response of the system. The visible emissions are very intense, although much narrower in wavelength than the other three features.

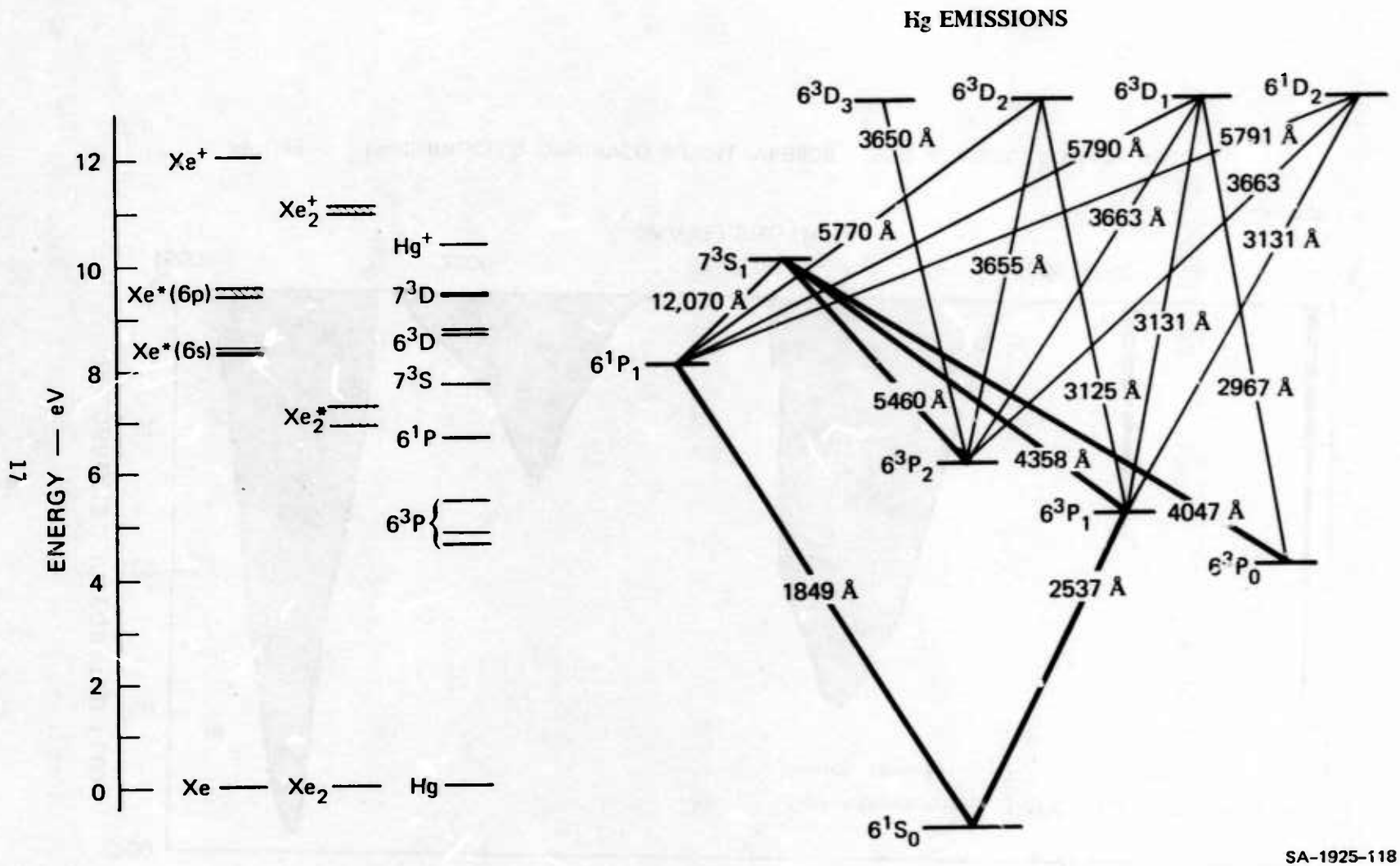

FIGURE 2 RELEVANT ENERGY LEVELS FOR THE Xe + Hg SYSTEM

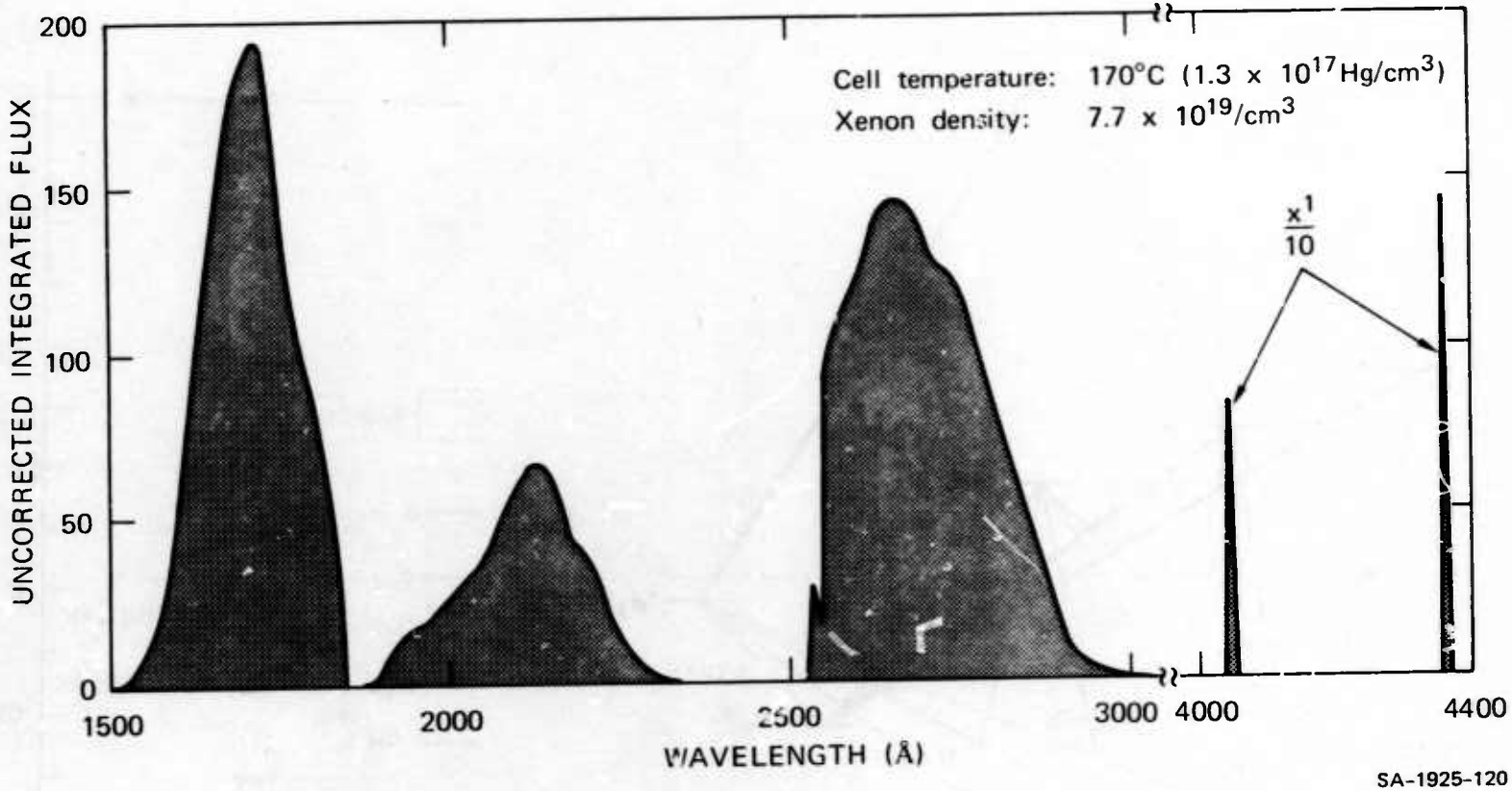

FIGURE 3 UNCORRECTED OBSERVED SIGNAL VERSUS λ FOR A MIXTURE OF Xe AND Hg

Perturbed 7^3S emissions

Emissions perturbed from the normal $Hg(7^3S\text{-}6^3P_{0,1,2})$ atomic transitions (at 4046 Å, 4358 Å, and 5460 Å) represent the second type of features observed. An example of these emissions is given in Figure 4. This is a microdensitometer trace of spectra taken on Polaroid film, which integrated the output of 100 excitation pulses, using a resolution of 0.4 Å. Although the figure is for the 4047 feature, the other two emissions have similar characteristics.

The structure is red-shifted by 1.5 Å from the atomic line, and has a second peak about 6 Å further to the red. The normal emission line cannot be seen, nor do we see a blue wing, but the intensities of the three 7^3S features are in the same ratio as the normal Hg emission lines. Also, the half widths of these emissions increase as the Xe pressure increases. This suggests that the radiation is shifted from the atomic line by a weak interaction with ground state xenon atoms.

Xe $Hg(6^3P)$ Excimer

The emission band peaking near 2700 Å is related to the Hg 6^3P levels. Figure 5 shows the time-integrated spectral output from a mix of 4650 torr Xe and 22 torr Hg at 210°C excited by 100 Febetron pulses. Figure 6 shows a synthesis of microdensitometer traces of three spectra taken at various exposures, showing more clearly the features. There are two satellite lines of the 2536.6 Hg line at 2529.5 Å and 2538.2 Å. Within the errors of our measurements, these are the same as the satellite lines appearing in emission, fluorescence, and absorption on the 2536 transition, as reported by Kielkopf and Miller [KM74]. The absence of the 2536.6 Å line is expected because of radiation trapping.

The wide band between 2550 Å and 3000 Å is a relatively more complex emission, also related to the 2536.6 feature. It is red-shifted from the $6^3P_1\text{-}6^1S_0$ transition and appears to have a regularly spaced lined structure

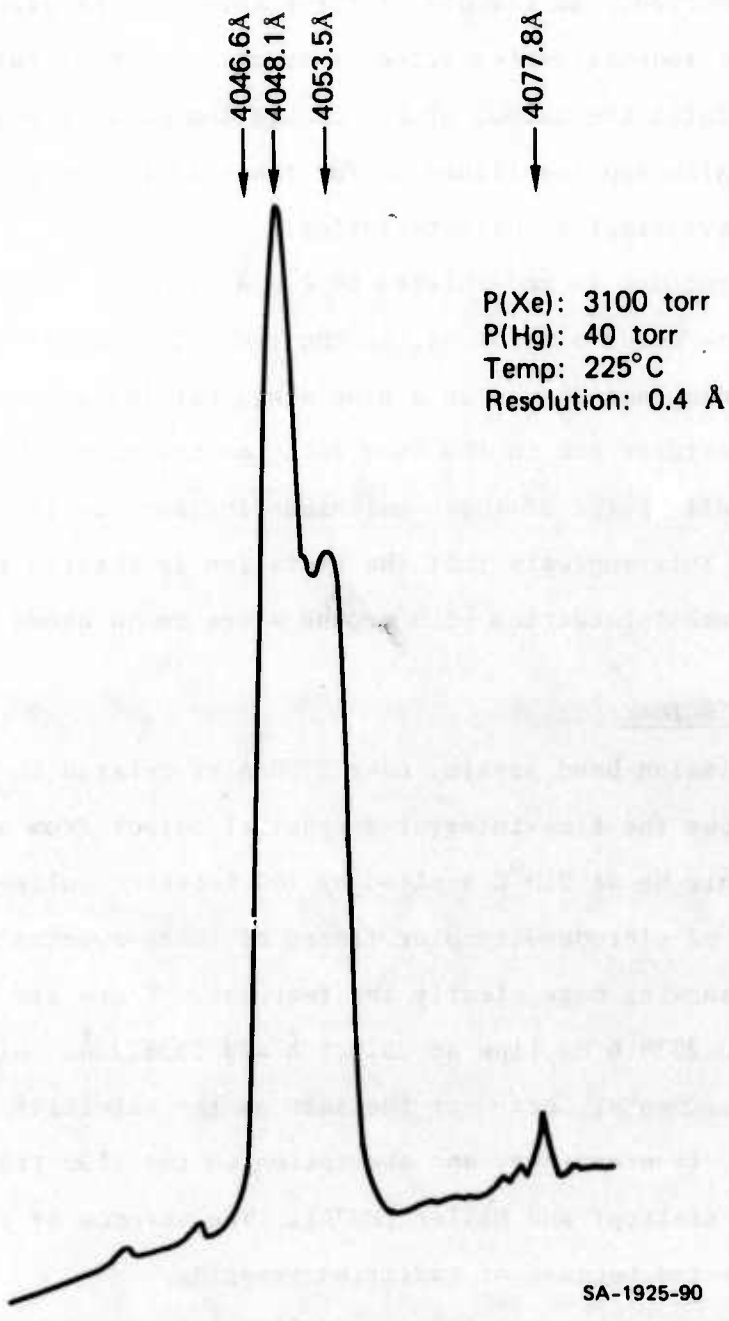

FIGURE 4 MICRODENSITOMETER TRACING OF THE PERTURBED Hg (7^3S-6^3P_o) EMISSION

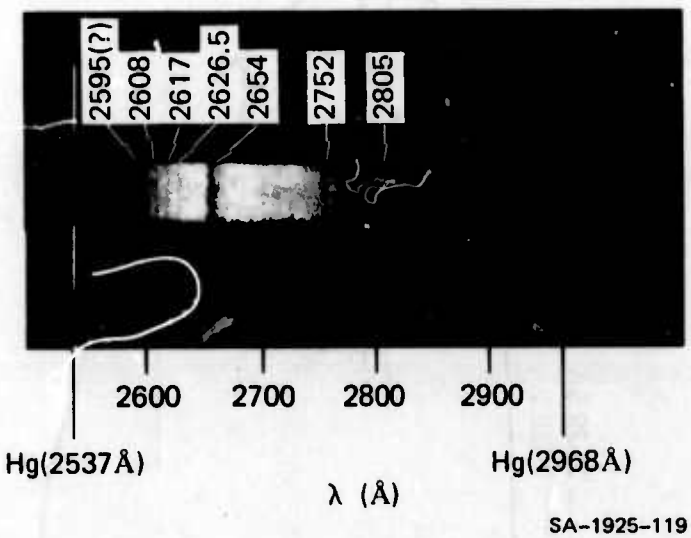

FIGURE 5 TIME INTEGRATED SPECTRUM OF EXCITED Hg-Xe MIXTURE, p(Xe) = 4650 torr AND T = 210°C

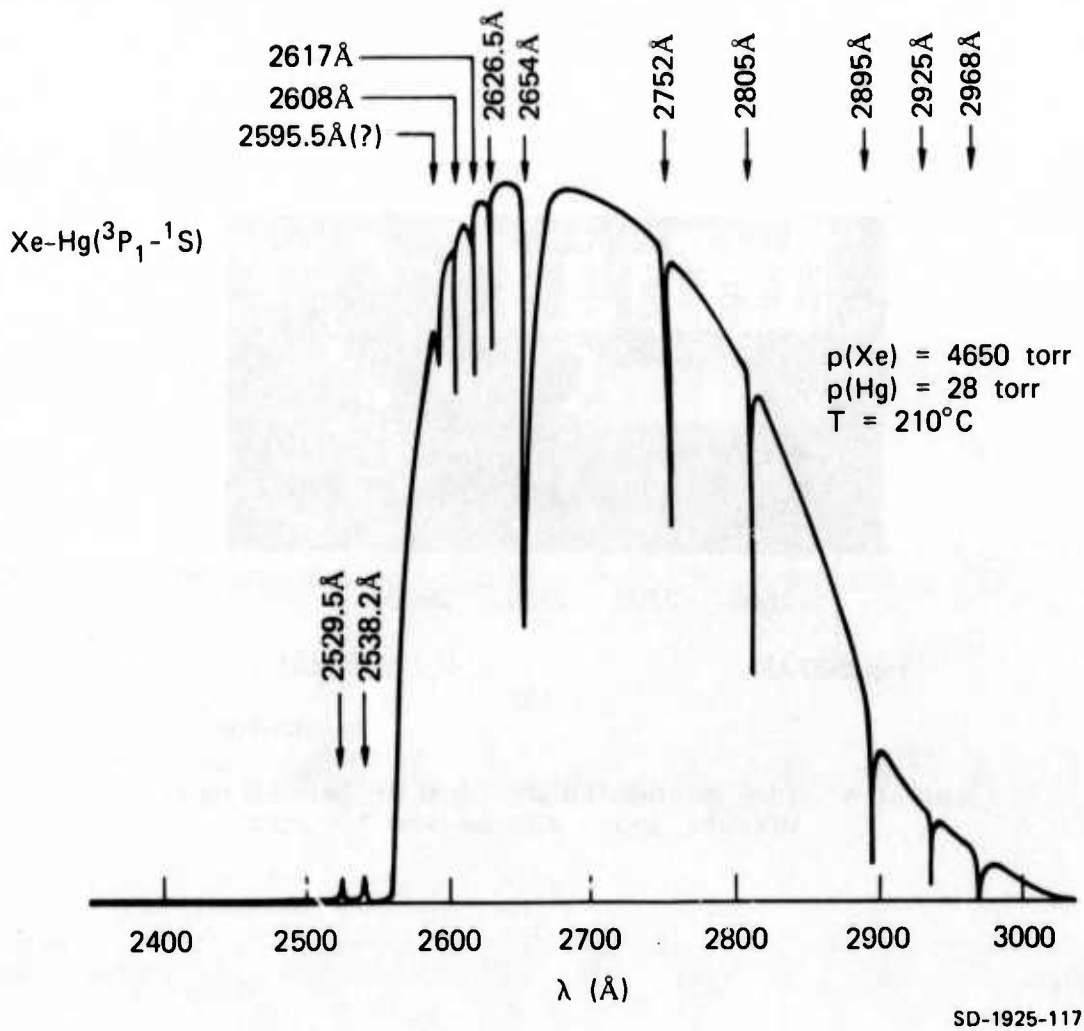

FIGURE 6 SYNTHESIS OF THREE MICRODENSITOMETER TRACINGS OF THE λ2700Å Hg-Xe EMISSION, USING A RESOLUTION OF 0.4Å

in the 2590 Å to 2626 Å region. It extends over a 400 Å range and contains absorption bands from the $^3P_{2,1}$ levels to higher excited Hg levels, e.g., the 6^3P_1-7^3D_1 transition at 2654 Å. Note that this absorption implies a very high population of Hg(^3P) states. Although the width of the absorbed line is about the same as for the 7^3S_1 emissions and has the same characteristic degradation to the red, it does not appear to be double peaked.

The shape of the broad band varies with the temperature and pressure of Hg. The structure between 2590 Å and 2626 Å disappears at higher temperatures, and the band's peak intensity decreases as the mercury partial pressures rise above 30 torr. The wavelength position of the peak intensity also varies with the Hg pressure, moving toward the blue as the pressure rises from 0.003 torr to 7 torr. This is illustrated in Figure 7. At pressures of Hg greater than 80 torr, the temporally integrated spectrum (Figure 8) gives the appearance of a broad band with emission spikes instead of the absorption lines shown in Figure 6. The time decay of these features has two components, the initial one corresponding to the direct excitation, and the final slope characteristic of the band decay itself. This suggests that there is transfer from the upper atomic xenon levels to upper Hg states, which emit before the 6^3P population begins to build to significant concentrations.

To find out if the regularly spaced features between 2590 Å and 2626 Å were due to absorption (which would imply a bound diatomic ground state with at least three vibration levels), we studied the absorption of Xe-Hg in the 2400 Å to 2700 Å region. Figure 9 shows our absorption profiles of the Xe-Hg system for various partial pressures of Hg and a Xe pressure of 1550 torr. We do not see any structure between 2580 and 2650 Å corresponding to the emission features of Figure 6. One of the satellite lines can be seen on the low wavelength side of the 2536.6 Å absorption peak. This set of curves is similar in appearance to those

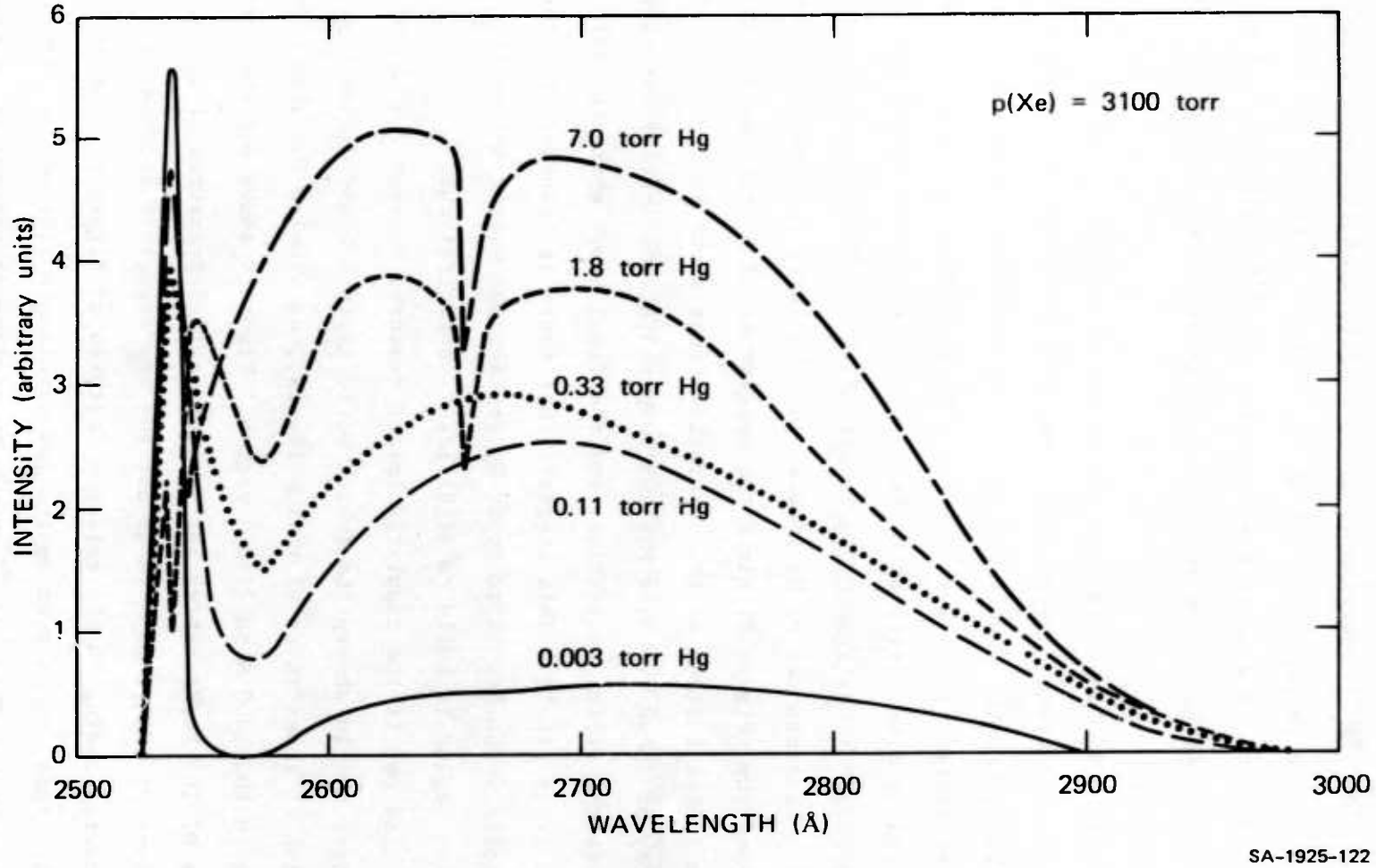

FIGURE 7 2700Å BAND PEAK INTENSITY VERSUS WAVELENGTH FOR VARIOUS Hg PRESSURES

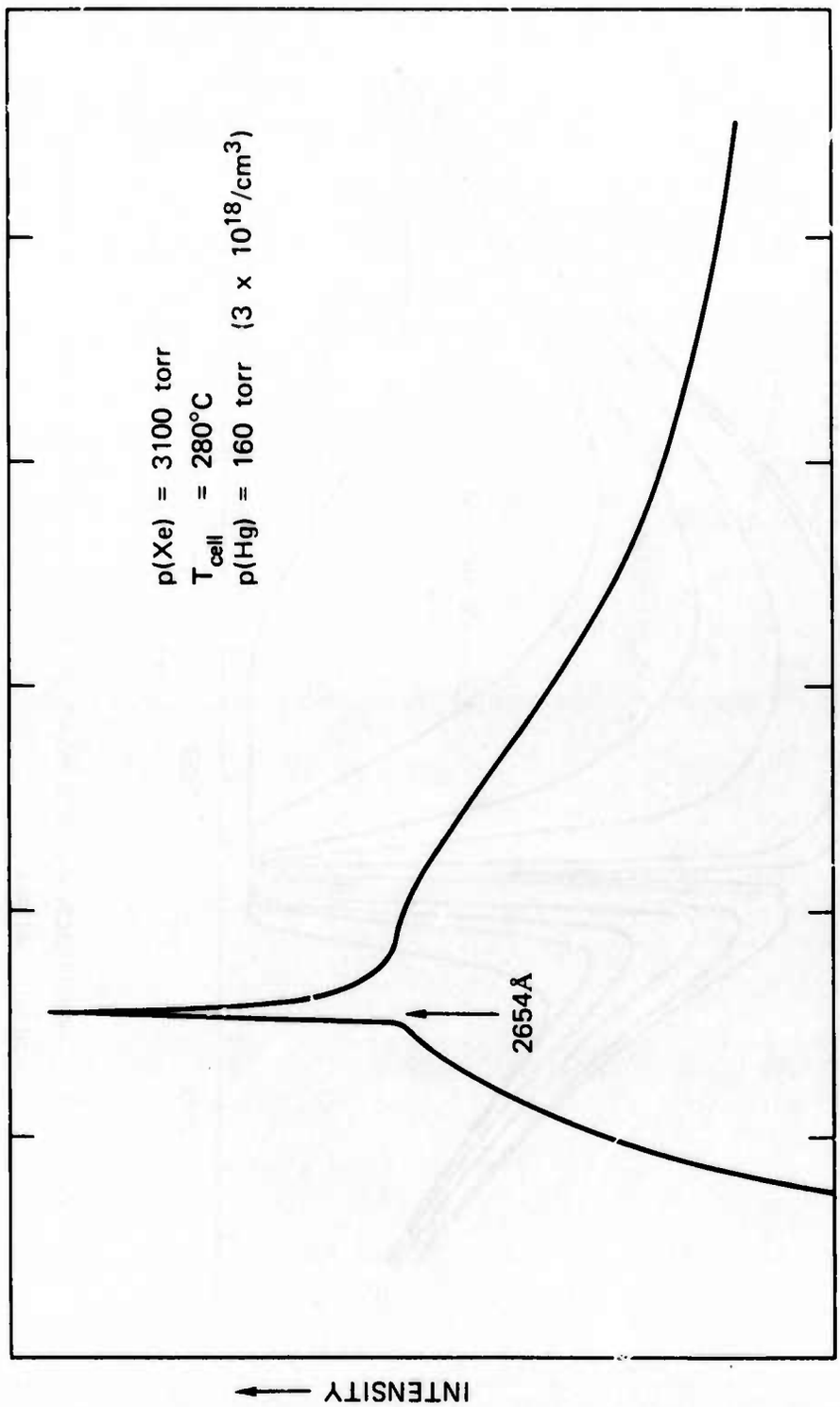

FIGURE 8 2700Å BAND PROFILE AT HIGH MERCURY PRESSURES, SHOWING DIRECT EXCITATION OF 2654 LINE

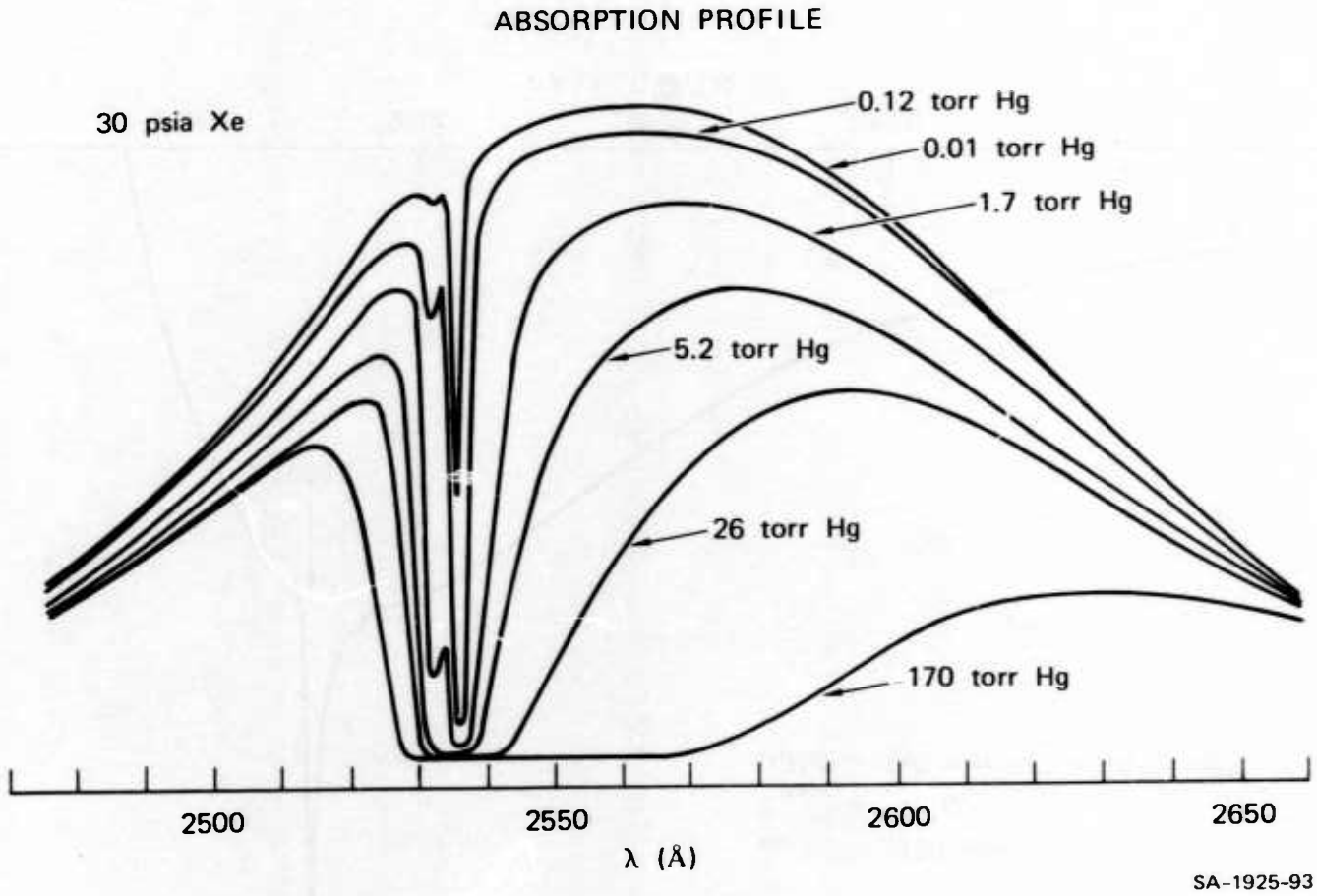

FIGURE 9 ABSORPTION CURVES NEAR 2537Å FOR VARIOUS MERCURY PRESSURES
p(Xe) = 30 psia.

obtained by Tanaka, et al. [TYF73] in their vuv absorption studies on Kr_2 van der Waals molecules and by Brewer, et al. [BMB65] in their examination of uv absorption spectra of Hg in low temperature (solid) rare gas matrices.

2100 Å Band

The fourth emission observed in our study was observed only by our photomultiplier system, since Polaroid film has very poor response to photons with wavelengths less than 2200 Å. The peak of the emission appears to be at 2125 Å and, as Figure 3 shows, has a width of about 200 Å. For our range of Hg and Xe pressures, this structure did not appear to shift its peak intensity nor to have any structured absorption or emission lines. It is assumed to be an excimer state formed from $Hg(6^3P_2)$ and a ground state xenon.

Xe_2 Excimer

The fifth emission band that was observed was the Xe_2^* excimer band centered at 1720 Å. One of the problems encountered in monitoring this vacuum ultraviolet emission, 1720 $\pm$ 100 Å, was the substantial absorption in the 1849 Å region due to the presence of Hg in the cell, even at room temperature. Although we could not take an absorption spectrum in the 1849 Å region similar to that which was taken at 2537 Å, work at Sandia Laboratories (Wo75) has shown the two to be similar.

Hg_2 Excimer

In a pure rare gas system, the incident energy of the e-beam is eventually observed as vuv emission from the excimer (for Xe, at 1720 Å). As Hg is added to the system, the rare gas excimer is replaced by a lower energetic excimer, $HgXe^*$, whose spectral emissions are at longer wavelengths (2100 Å and 2700 Å). As Hg attains higher partial pressures, we see these uv emissions decrease, implying that the $HgXe^*$ excimer is being

replaced by an even lower energetic excimer, the Hg_2^* dimer (or Hg_3^* trimer). At sufficiently high Hg pressures (760 torr), we have measured these emissions (e.g., 3300 Å) and have observed that they become brighter as the $HgXe^*$ bands decrease in intensity.

Temporal Behavior

We shall briefly present the results of our time-dependent measurements here and then shall discuss them in detail in the next section. The first observation that can be made is that the decay times of the Xe_2 band and of the 7^3S emissions are remarkably similar when the natural radiative lifetime of the sodium salicylate (12 ns) [Sam67] is taken into account. If an incident light pulse (photons/sec) of the form $Ae^{-\nu t}$ strikes the sodium salicylate surface, the number of "stored photons" X in the scintillator can be described by

$$\frac{dX}{dt} = \epsilon A e^{-\nu t} - \nu_r X$$

where $1/\nu_r = \tau_r$ is the sodium salicylate natural radiative lifetime, and ϵ is the efficiency of conversion. The solution of this differential equation is

$$X = \frac{\epsilon \nu N_{tot}}{\nu_r - \nu} \left(e^{-\nu t} - e^{-\nu_r t} \right)$$

where N_{tot} is the integrated number of photons striking the surface. The observed intensity will just be $\nu_r X$. The measured decay frequency ν_m (as measured during the first 200 ns of decay) will be slower than the real decay frequency ν, when ν is close to ν_r, and, of course, will never be faster than ν_r. Figure 10 shows this relationship for ν versus ν_m using a value of $\tau_r = 12$ ns.

For our measurement, the sodium salicylate will fluoresce when exposed to the 1720 Xe_2 excimer emission but be transparent to the 7^3S emission at 4047 and 4358. For decay times close to the radiative lifetime

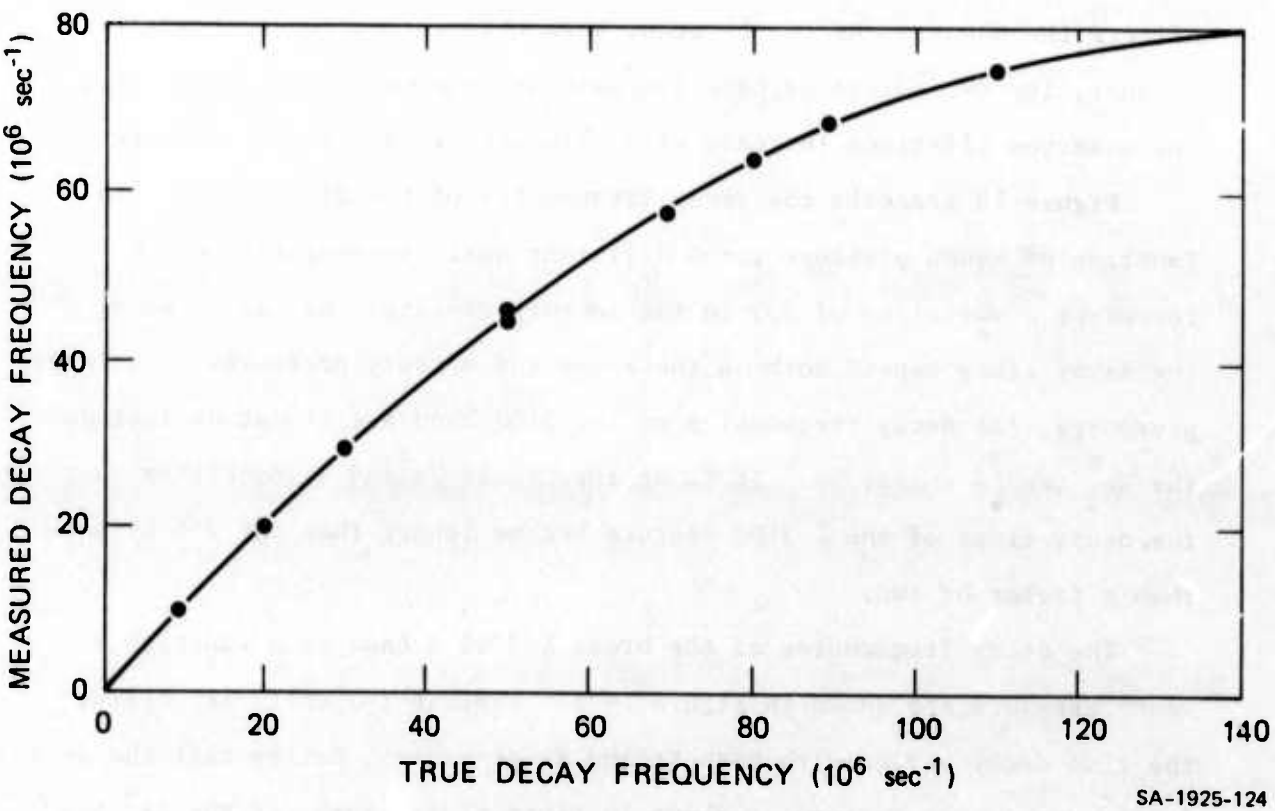

FIGURE 10 EFFECT OF SODIUM SALICYLATE RADIATIVE LIFETIME (τ_R=12 ns) ON MEASURED DECAY FREQUENCIES

of the scintillator, the resulting time decays of the 1720 Å band should then be slower than for the 7^3S emissions. This is in fact what we observe. Figure 11 displays the decay frequencies of the 7^3S emissions as a function of xenon pressure for various mercury densities. Similar decay frequencies were observed for all three 7^3S emissions. Figure 12 displays the corresponding decay frequencies observed for the Xe_2^* band and shows the corrected values for the cases of 1.5×10^{18} and 3.7×10^{17} Hg/cm^3, the only ones in which the salicylate lifetime significantly affects the decays. As can be seen, when this correction is taken into account, the two emissions have the same decay frequencies. Note that the observed lifetimes increase with both mercury and xenon pressure.

Figure 13 presents the decay frequencies of the 2100 Å band as a function of xenon pressure for 4 different cell temperatures, which represent a variation of 200 in the mercury density. As can be seen, the decay times depend both on the xenon and mercury pressures. At lower pressures, the decay frequencies of the 2100 band are almost as fast as the Xe_2^* or 7^3S emissions. It is at the higher Xe and Hg densities that the decay times of the λ 2100 feature become longer than the 7^3S by more than a factor of two.

The decay frequencies of the broad λ 2700 Å band as a function of xenon pressure are shown in Figure 14 for various temperatures. Again, the time decay varies with both Xe and Hg pressure. Notice that the decay frequency of this feature is about 10 times slower than for the Xe_2^* band, but that it too seems to vary linearly with the xenon pressure.

Intensity Variations

We can now describe the variation of intensity with the pressure and temperature. The most useful quantity is an actual measure of the photon flux, that is, the time and wavelength integrated output of the total band for a given Febetron excitation pulse. This quantity, when multiplied by the proper geometrical and calibration factors, can give the integrated photon flux per unit volume in the excitation region.

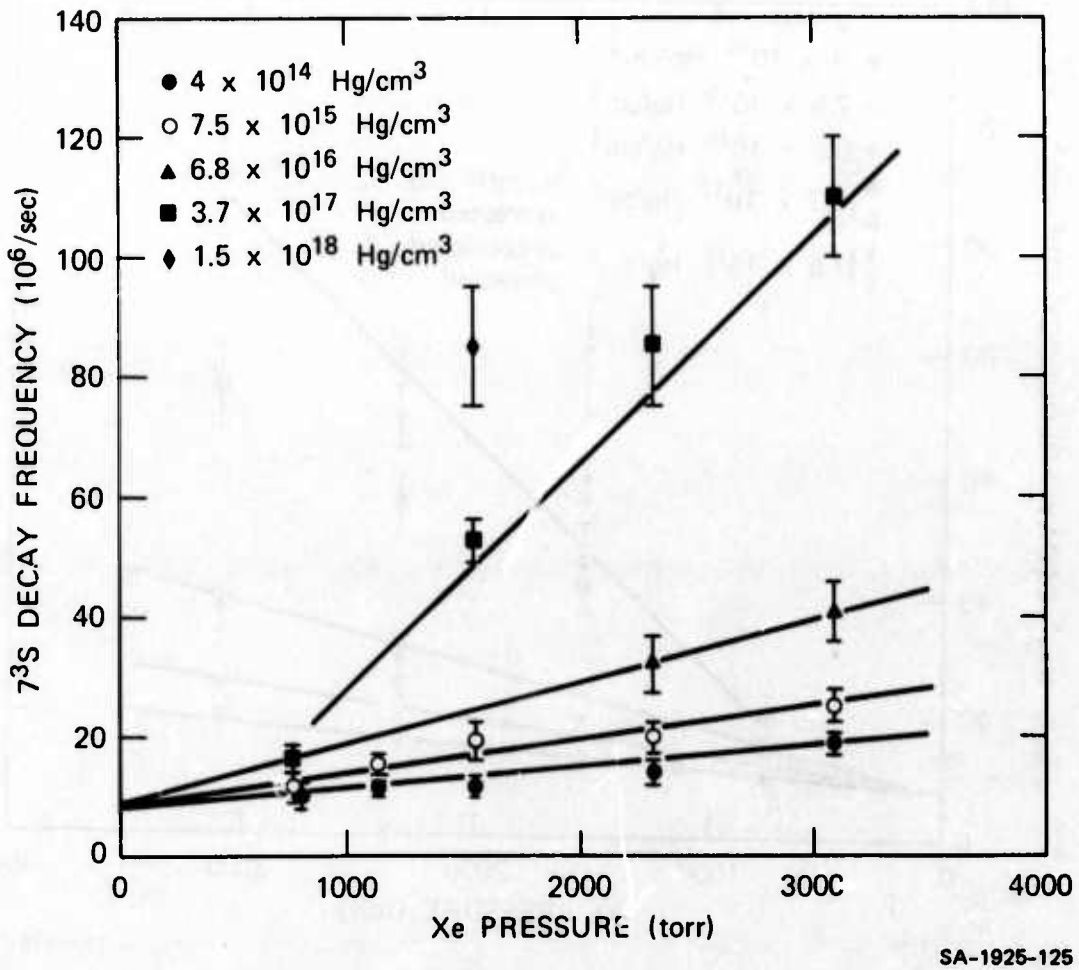

FIGURE 11 Xe-Hg (7^3S) DECAY FREQUENCY VERSUS Xe PRESSURE FOR VARIOUS Hg DENSITIES

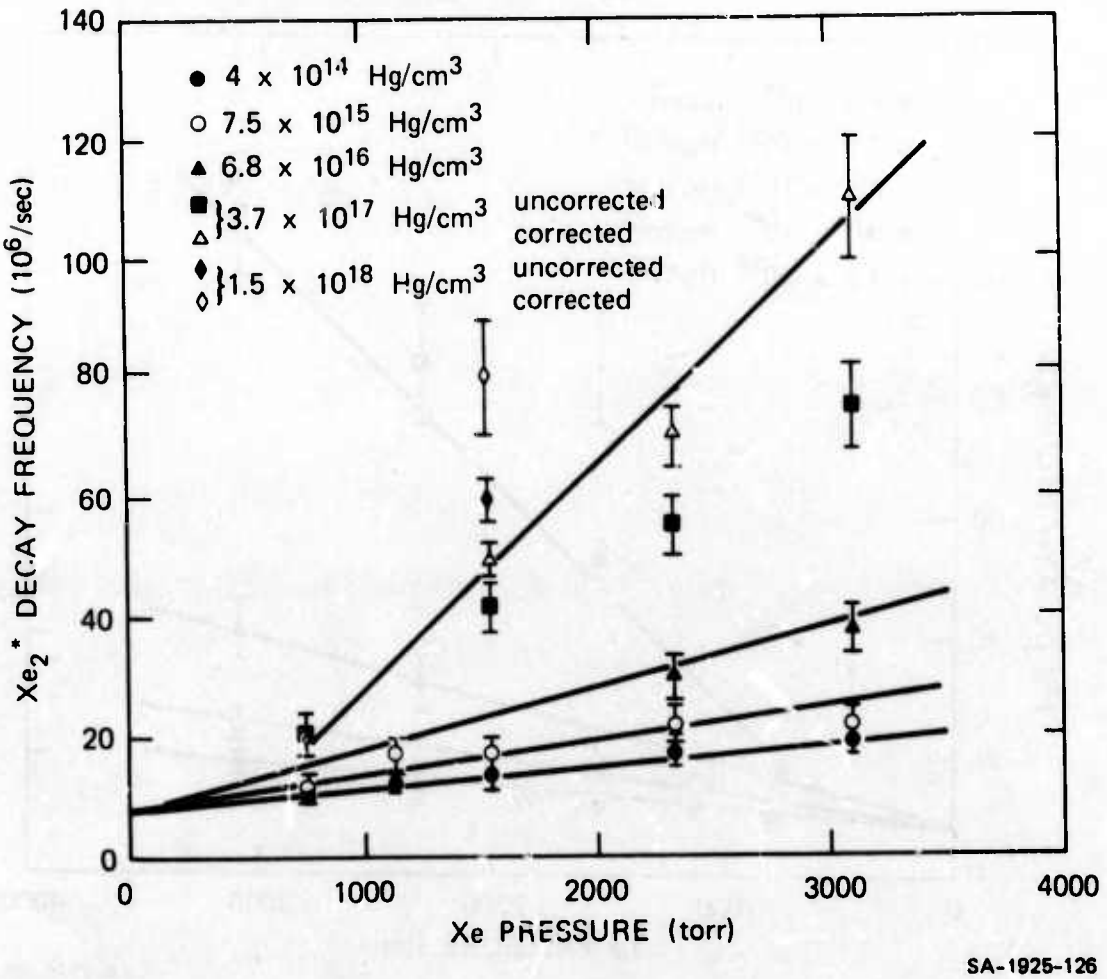

FIGURE 12 Xe_2^* (1720Å) DECAY FREQUENCY VERSUS Xe PRESSURE FOR VARIOUS Hg DENSITIES

The higher values are corrected for the sodium salicylate radiative lifetime.

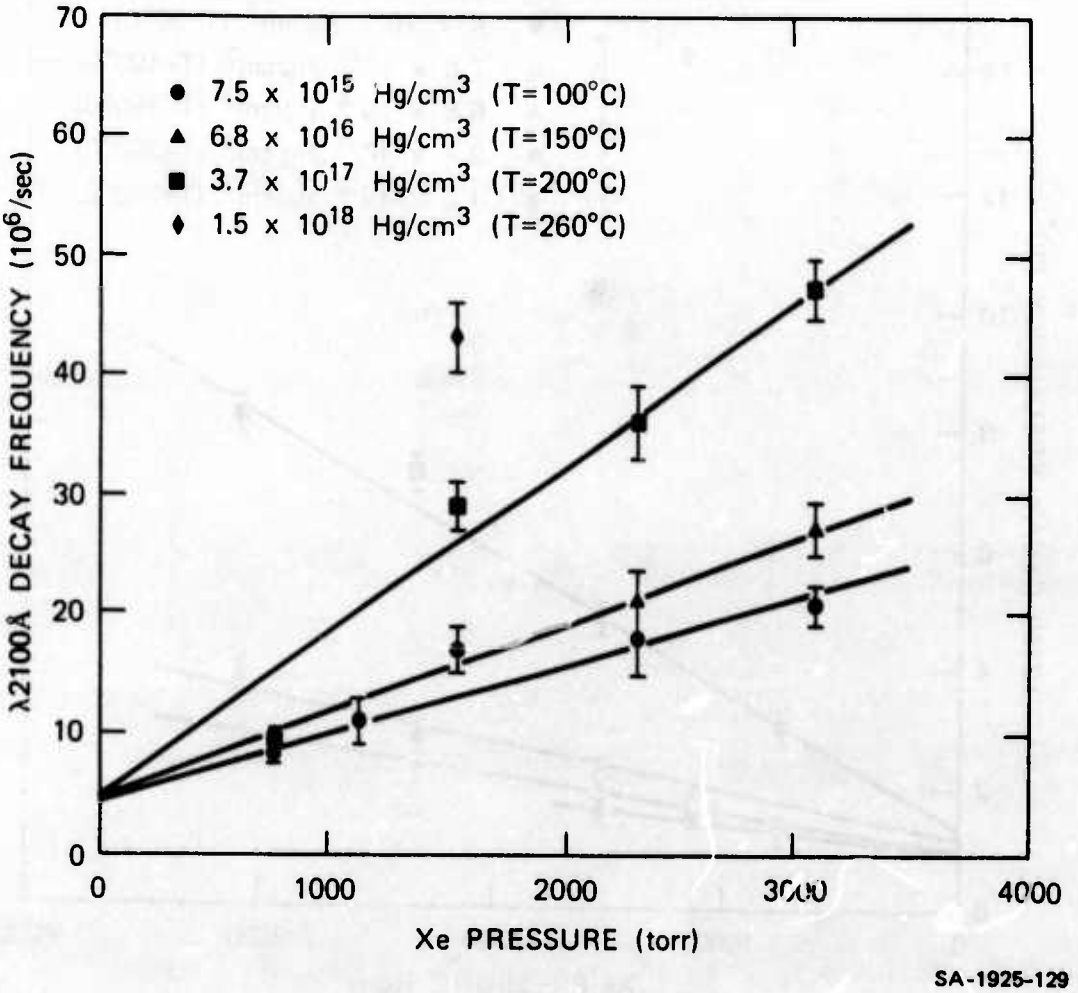

FIGURE 13 λ2100Å BAND DECAY FREQUENCY VERSUS XENON PRESSURE FOR VARIOUS Hg DENSITIES

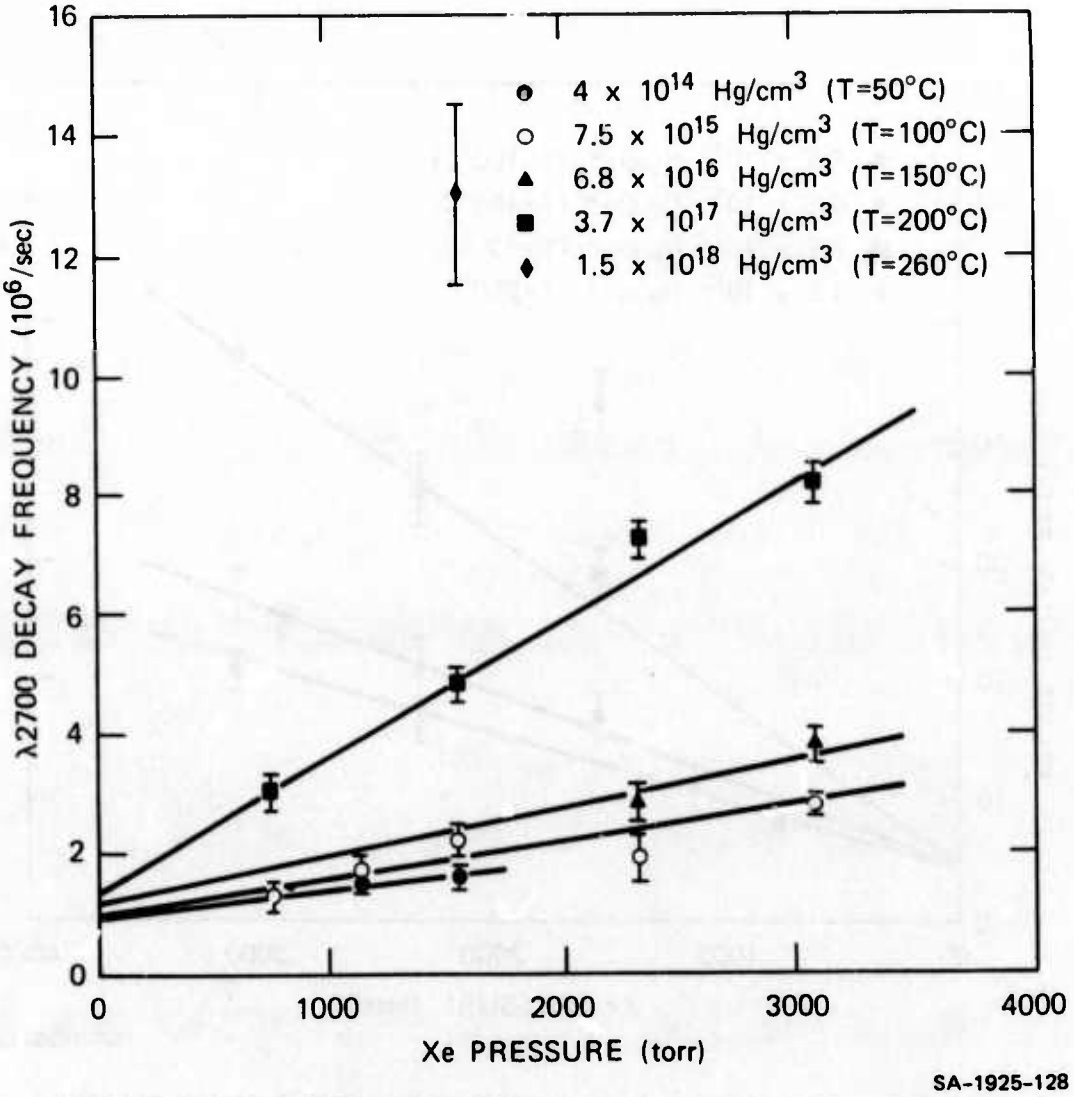

FIGURE 14 λ2700Å BAND DECAY FREQUENCY VERSUS XENON PRESSURE FOR VARIOUS Hg DENSITIES

An example of a measurement of the integrated photon flux described above is given in Figure 15, where the 1720 Å band output (peak signal multiplied by the decay lifetime) is plotted against Hg density for various xenon pressures. Notice that as the Hg density increases, the amount of energy actually released by excimer emissions becomes less, indicating the energy path is now directed through another channel. This is in agreement with our observations of the Xe-Hg photon fluxes (i.e., 2100, 2700, 4048, 4358, and 5460 Å), which increase with mercury density as the Xe_2^* emissions decrease.

Fluorescence Yield

We can compute the fluorescence yield of each of the Hg-Xe emissions by folding in the calibration factors, and dividing the observed photon flux by the original integrated flux that was observed in the Xe_2^* channel (1720 Å) with no Hg present. These values, which represent the percentage of photons that come out in each of the bands compared with the total number that was originally measured are presented in Table I and in the next four figures. In Figure 16(a), the yield for the λ2100 Å band can be seen to vary between 1/2 and 4-1/2%, the lowest in value of the three Hg-Xe emissions. Within experimental error, the yield seems to be fairly constant with respect to xenon pressure, but varies with Hg pressure, being the highest in the neighborhood of 3.7×10^{17} Hg/cm^3 (about 200°C or 20 torr vapor pressure).

Figure 16(b) shows that the λ 2700 emission represents a much higher fluorescence yield, varying in our measurements between 1 and 23%. The yield seems to increase slightly with xenon pressure, but has the highest value for Hg densities between 1 and 4×10^{17} atoms/cm^3.

In Figure 17(a), the 7^3S fluorescence yields are presented as a function of xenon pressure for 4 different mercury densities. Here we see the opposite behavior with respect to xenon pressure compared to the

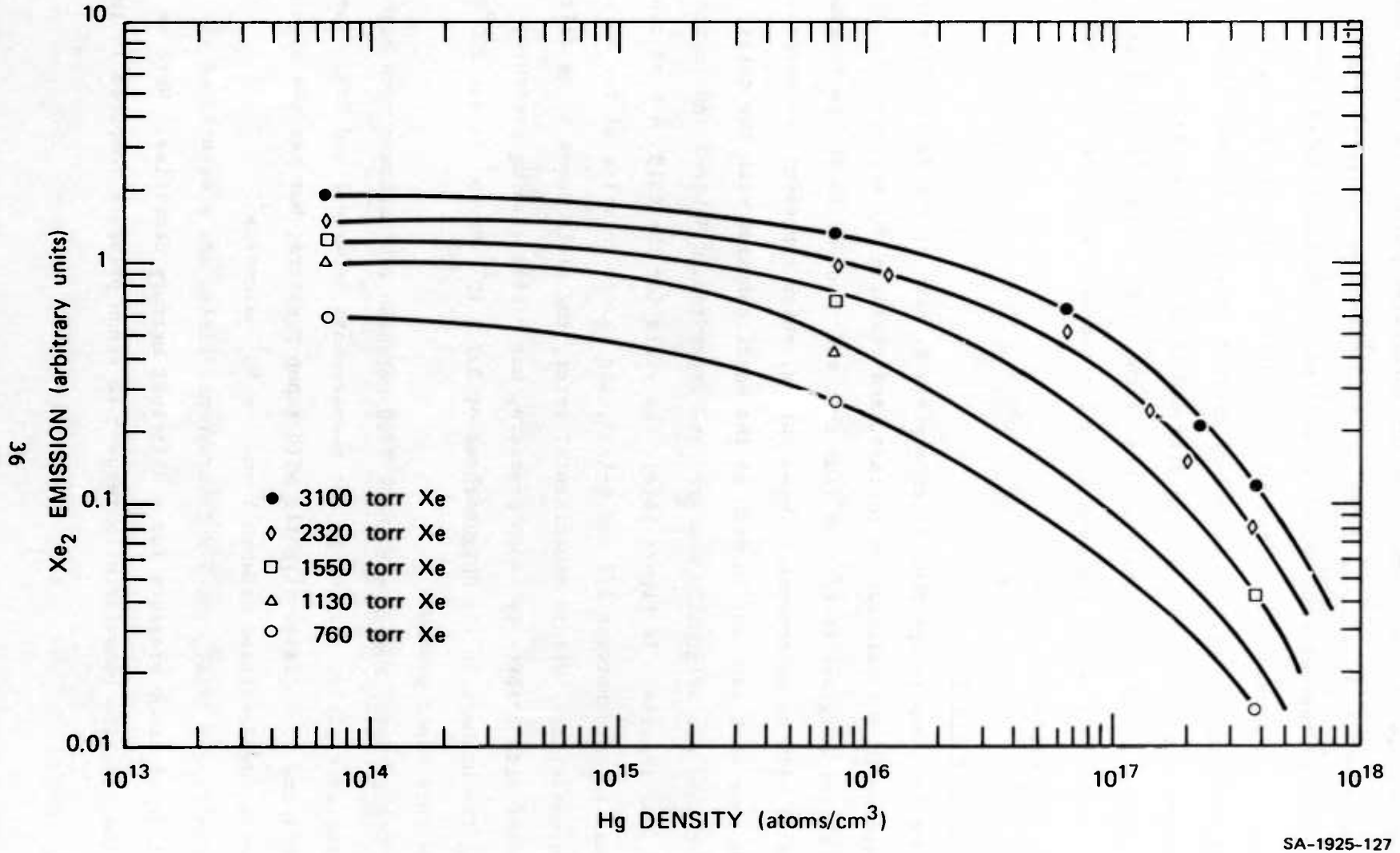

FIGURE 15 Xe_2 EXCIMER INTEGRATED PHOTON FLUX VERSUS Hg NUMBER DENSITY FOR VARIOUS Xe PRESSURES

Table I

FLUORESCENCE YIELD CALCULATIONS

P(Xe) (torr)	[Hg] (atoms/cm^3)	Temp (^oC)	Xe_2^*	λ2100	λ2700	7^3S
760	7.5(15)	100	45%	1.7%	20	12
	3.7(17)	200	2.2	4	10	24
1130	7.5(15)	100	40	1.6	16	10.5
1550	7.5(15)	100	60	1.2	14	7.2
	3.7(17)	200	3.8	2.8	10	13
	1.5(18)	260	0.3	0.46	1.6	9.3
2320	7.5(15)	100	65	-	-	7.6
	6.8(16)	150	34	-	-	12
	3.7(17)	200	5.5	3.5	15	11
3100	7.5(15)	100	70	1.35	20	2.8
	6.8(16)	150	34	3.5	23	7.6
	3.7(17)	200	6.3	4.5	14	6.3

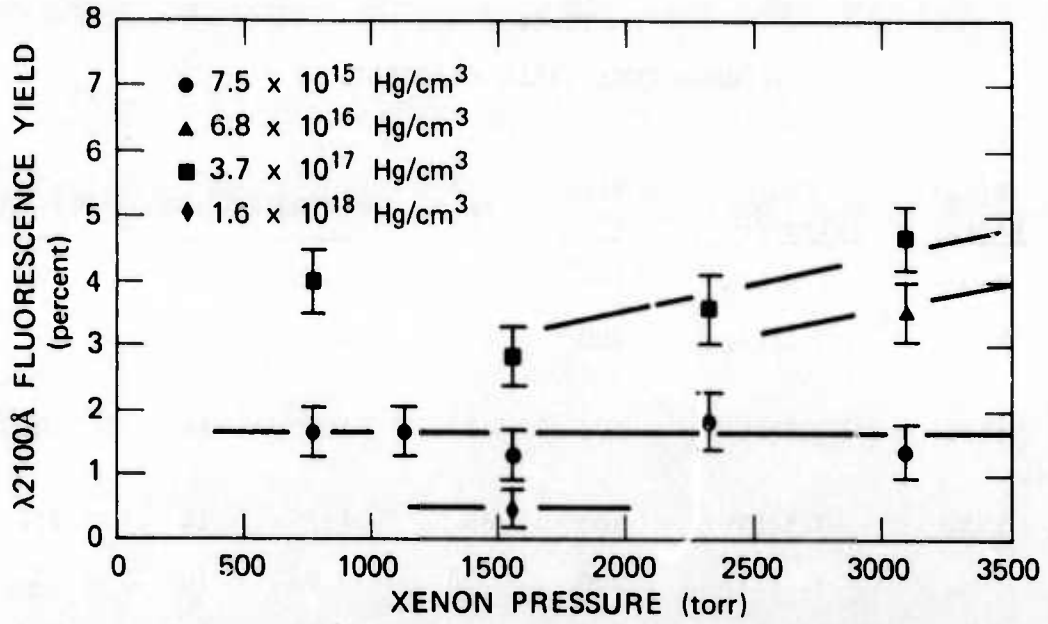

(a) λ2100Å FLUORESCENCE YIELD VERSUS XENON PRESSURE FOR VARIOUS MERCURY DENSITIES

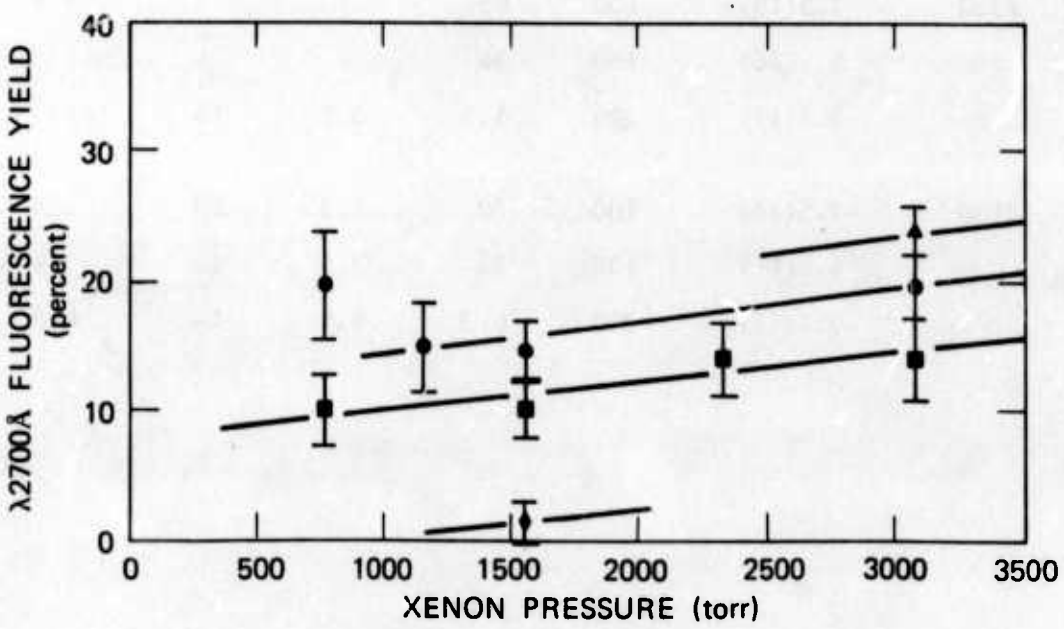

(b) λ2700Å FLUORESCENCE YIELD VERSUS XENON PRESSURE FOR VARIOUS MERCURY DENSITIES

SA-1925-130

FIGURE 16

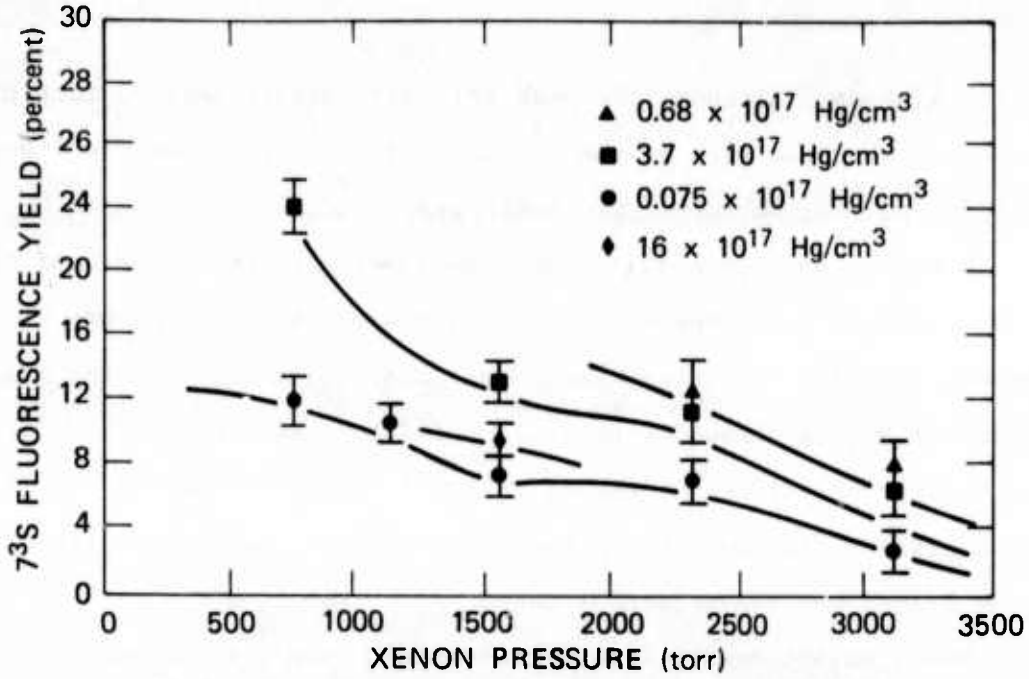

(a) 7^3S FLUORESCENCE YIELD VERSUS XENON PRESSURE FOR VARIOUS Hg DENSITIES

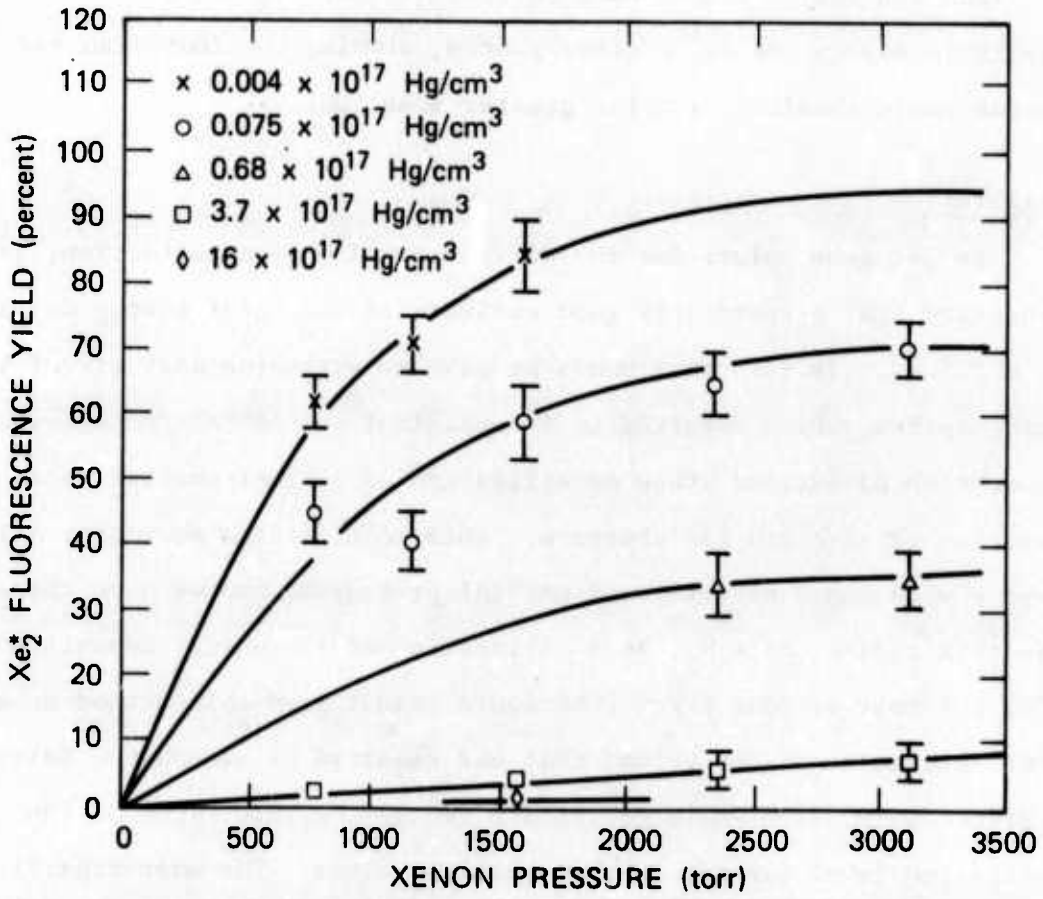

(b) Xe_2^* 1720Å FLUORESCENCE YIELD VERSUS XENON PRESSURE FOR VARIOUS Hg DENSITIES

SA-1925-131

FIGURE 17

λ 2700 Å bands. Although the peak intensity occurs near 20 torr of mercury, the rapid rise of the 7^3S decay frequency causes the fluorescence yield to be maximum for Hg pressures near 3 torr.

Finally, in Figure 17(b), we show the fluorescence yield of the Xe_2 1720 band. It decreases with increasing amounts of Hg, as one would expect, but it also varies with xenon pressure, increasing for a given amount of Hg, in direct contrast to the 7^3S emissions, which decrease. For low Hg concentrations the majority of energy is emitted via the Xe_2^* vuv radiation, but when the pressure of added Hg is above a few torr, the Hg-Xe states are the major emitters.

These magnitudes of fluorescence yield seem reasonable. At most, all our errors could change the values by 50%. Note that since a 7^3S emission and one of the uv band photons (either 2100 Å or 2700 Å) together equals in energy one Xe_2^* excimer photon, summing the four fluorescence yields could result in a value greater than 100%.

Calibration of Excitation

To get good values for the efficiency of photon collection, it is necessary that a reasonably good estimate of the total energy deposited be obtained. In reference HGH74 we gave an extensive analysis of the Ar/N_2 system, which resulted in a consistent set of rate constants for production of excited state densities and of photons emitted as a function of time and gas pressure. This model fitted our observations over a wide range of total and partial pressures, and we have chosen to use this system, $Ar + N_2$, as a calibration of the energy deposition.

The most serious error that could result from this method would be a misestimation of the volume that was observed by our photon detection system. This error would contribute to the absolute value of the excitation level but not to the relative values. The most significant error in the estimate of the relative values would come about from our

calibration of the sensitivity of the optical detection system as a function of wavelength as outlined in the experimental section. We estimate that both these errors could be as large as 50%.

This calibration technique can be used to check the excitation in the xenon-mercury cell in the following way. We can measure the total number of emitted photons in the N_2 2+ system as well as the total number of photons emitted by the Xe_2^* excimer band. At 2 atmospheres in our original rare gas cell, the model predicts the following: 2.2×10^{15} Ar excitations per cm^3, 7.5×10^{14} total number of excitations produced in the N_2C state, and 2.0×10^{14} photons per cm^3 actually emitted. For xenon at 2 atmospheres in the same cell we observed a total integrated flux in the Xe_2^* excimer band of 9.8×10^{15} photons/cm^3 [HGH75]. The ratio of the Xe_2^* emission to the N_2 2+ emission is then $9.8 \times 10^{15} \div 2.0 \times 10^{14}$, which is equal to 48. This same ratio measured in the Xe-Hg cell is $1.15 \times 10^{15} \div 2.3 \times 10^{13}$, which is equal to a ratio of 50, showing that our calibrations for the two systems are consistent within about 5%. It also indicates that if our estimates of the excitation volume in the two cases is accurate, the amount of deposited energy in the xenon-mercury cell is a factor of 8.6 times lower than in the rare gas cell.

D. Data Analysis

We are attempting to find a dynamic model for the mixed excimer (mercury-xenon) system, which should explain the main features of the experimental results and allow for predictions of such characteristics as fluorescence yield and overall behavior as a function of temperature and pressure.

The principal experimental results, which must be compatible with our model, are

(1) The apparent coupled behavior of Xe_2^* radiation and the 7^3S radiations from Hg,

(2) The shape of the band structures radiated near the normal atomic 7^3S lines, and

(3) The spectrum of the 2100 Å and 2700 Å excimer radiations, and, in particular, the temporal and intensity variations of these bands as a function of mercury and xenon pressure.

(4) The fluorescence yield.

To get a feeling for the requirements of the model we must understand where the energy that is deposited by the electron beam flows. We suggest the simplified energy flow diagram shown in Figure 18. Approximately 50% of the initial energy deposited goes into the general heating (LO72) and the rest creates excited states and ions of the rare gas. Models of the rare gas excimer formation [WGH74, LEH73] have shown that the formation of the rare gas metastable and the subsequent excimer formation is very rapid at pressures of several atmospheres (Reactions 1-5, Table II). Since the electron temperature is on the order of tenths of an eV, the singlet and triplet excimer states are mixed, causing the observed lifetime of the (vuv) excimer radiation to be a

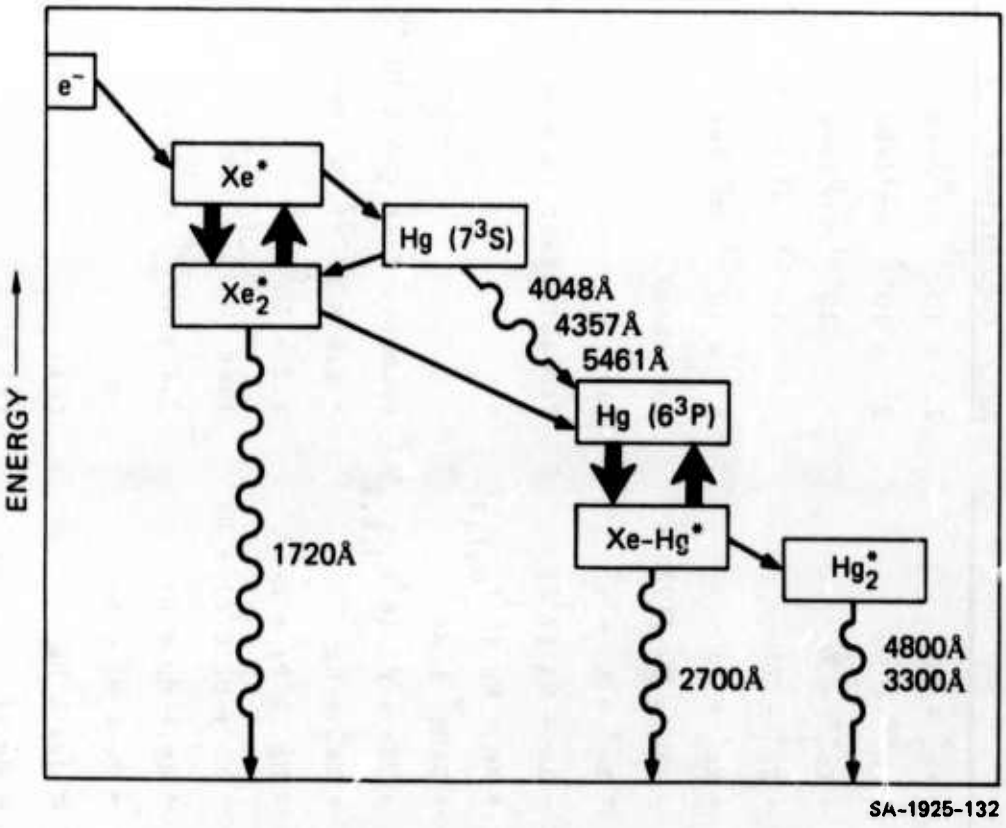

FIGURE 18 ENERGY FLOW DIAGRAM OF THE XENON-MERCURY SYSTEM

Table II

REACTIONS AND RATES IN XENON-MERCURY SYSTEM

Reaction No.	Reaction	Rate Coefficient	Reference
1	$Xe^+ + 2Xe \rightarrow Xe_2^+ + Xe$	2.5×10^{-31} cm^6/sec	Ma65,McD70,SDP72
2	$Xe_2^+ + e^- \rightarrow Xe^{**} + Xe$	2×10^{-7} cm^3/sec	BB70
3	$Xe^{**} + 2Xe \rightarrow Xe_2^{**} + Xe$	10^{-31} cm^6/sec	LEH73
4	$Xe_2^{**} + Xe \rightarrow Xe^* + 2Xe$	10^{-11} cm^3/sec	LEH73
5	$Xe^* + 2Xe \rightarrow Xe_2^* + Xe$	5×10^{-32} cm^6/sec	BoM70,KFR74
6	$Xe_2^* \rightarrow 2Xe + h\nu$ (1720 Å)	Variable	LEH73
7	$Xe_2^* + e^- \rightleftharpoons Xe^* + Xe + e^-$	(a)	
8	$Xe^* + Hg \rightarrow Xe + Hg\ (7^3S)$	Probably fast ($\sim 5 \times 10^{-10}$ cm^3/sec)	estimate
9	$Xe^* + Hg \rightarrow Xe + Hg\ (6^3P_{0,1,2})$	-	
10	$Xe_2^* + Hg \rightarrow XeHg^* + Xe$	-	
11	$Xe_2^* + Hg \rightarrow 2Xe + Hg\ (6^3P_{0,1,2})$	Probably fast ($>5 \times 10^{-10}$ cm^3/sec)	estimate
12	$2Xe + Hg(7^3S) \rightarrow Xe_2^* + Hg$	$> 1.6 \times 10^{-32}$ cm^6/sec	present work
13	$Hg\ (7^3S) \rightarrow Hg\ (6^3P) + h\nu$	1.2×10^8 s^{-1}	HP74,BCL65
14	$Xe + Hg(7^3S) \rightarrow Xe + Hg(6^3P) + h\nu$	fast ($> 10^{-14}$ cm^3/sec)	estimate
15	$Xe + Hg(6^3P) \rightarrow Xe + Hg + h\nu$	2.1×10^{-14} cm^3/sec	present work
16	$Xe\text{-}Hg^* \rightarrow Xe + Hg + h\nu$	-	
17	$Xe\text{-}Hg^* + Xe \rightleftharpoons 2Xe + Hg\ (6^3P)$	(a)	
18	$Hg(6^3P_0) + Xe \rightleftharpoons Hg\ (6^3P_1) + Xe$	(a)	
19	$Xe\text{-}Hg^* + Hg \rightarrow Hg_2^* + Xe$	Probably fast	estimate

[a]Because the equilibrium constants are not known, these rates have not been derived.

complex function of the pressure [LEH73]. We also believe that this hot electron swarm establishes an equilibrium between Xe_2^* and Xe^* (Reactions 5 and 7).

The energy levels of the mercury-xenon system shown in Figure 2 indicate that only the xenon metastable can transfer energy to the mercury 7^3S excited state (Reaction 8), whereas both the metastable and the xenon excimer can transfer to the 6^3P system of mercury (Reactions 9 and 11). Since Xe^* is coupled to Xe_2^*, we can understand how $Hg(7^3S)$ is coupled to Xe_2^*.

There are two routes for the energy to go in this first step. The Xe_2^* can radiate to the repulsive ground state (Reaction 6, which, for our purposes, should be considered as energy lost) or the excitation energy can be transferred from the xenon metastable or excimer, ending ultimately in the 6^3P metastable levels of mercury. This can be reached by direct excitation (Reactions 9 and 11) or by cascade radiation from the 7^3S level (Reaction 13). The radiation from these excited atomic levels is trapped within the high pressure gas since they are unable to radiate directly to the atomic ground state. Bound radiating excimer states, however, can be formed with ground state xenon atoms. Bound levels formed from the $Hg(^3P_1)$ and $Hg(^3P_2)$ states should both be radiatively allowed since the normal triplet-singlet rule forbidding this transition is broken down by the large spin-orbit splitting. Because radiation from the $^3O^-$ excimer state formed from the $Hg(^3P_0)$ is forbidden by symmetry selection rules, it probably does not contribute to the observed emissions.

Radiation out of the $HgXe(6^3P)$ excimer states gives rise to the 2700 and 2100 Å bands. An additional collisional process, $Xe\ Hg^* + Hg \rightarrow Hg_2^* + Xe$ (Reaction 19), permits the energy to flow to the mercury excimers that radiate much more slowly in the bands from 3000 to 4800 Å. This process will be considered a loss term for the purposes of our model. The time decay of the 2700 Å band is then determined by the radiation

rate from the Xe Hg excimer level, the ratio of the atomic state population to the excimer population, and the rate of formation of Hg_2 excimers.

The lack of detailed measurements separating mercury pressure and temperature prevents us from making this model completely quantitative. The model does seem, however, to qualitatively fit the observations made and, therefore, by assuming this kinetic picture, we are able to derive some rate constants. Let us now examine this simplified picture in more detail and see how well it matches the experimental data discussed earlier.

Xe Excited States and Hg 7^3S

The data shown in Figures 11 and 12, when corrected for the response time of the sodium salicylate vuv detector, suggest that the Xe_2 excimer and the Hg 7^3S states are strongly coupled. The decay times show virtually identical behavior, and in addition, the lifetime observed for each radiation is a function of both the xenon pressure and the mercury density. The behavior of the xenon excited states in the pure rare gas under high pressure and high excitation density conditions has been studied fairly extensively [WGH74]. The pertinent reactions and suggested rate coefficients are shown in Table II. The best available model for the behavior of the rare gas excimer involves the collisional equilibrium produced between the Xe_2^* excimer and the Xe^* metastable levels by the low energy (0.2 to 0.4 eV) electrons remaining after the initial electron beam excitation. Sufficient electrons, $> 10^{13}/cm^3$, are available to produce this mixing after the original beam pulse has ended. It is this effect which is thought to lead to the observed dependence of the Xe_2 radiative lifetime on pressure and excitation conditions [LEH73, HGH75].

An additional feature in our case is the apparent strong coupling between the excited states in the Xe system and the 7^3S excited state in

Hg. The relevant energy levels shown in Figure 2 indicate that only the Xe atomic metastable can transfer to the 7^3S state of mercury, and furthermore that this state is unlikely to transfer energy back to the Xe metastable since the Hg 7^3S is at least 5000 cm^{-1} below the nearest Xe metastable. We could postulate, therefore, that the 7^3S would follow the vuv Xe_2^* radiation, which is in equilibrium with the atomic metastables. This conjecture founders on the data shown in Figure 4. It indicates there is little if any radiation occurring directly on the atomic line, due to the high density of the 6^3P states effectively trapping the atomic radiation. Therefore, the 7^3S level can radiate only when perturbed by a collision with a xenon atom. If we assume that the "collision" leading to the radiation has a cross section of 10^{-15} cm^2, then a simple calculation shows that each 7^3S mercury spends approximately 1% of the time in collision. This, however, would increase the apparent radiative lifetime by a factor of 100, which is much longer than the observed decay rate for the 7^3S levels. We must conclude, then, that the 7^3S transfers energy back into the Xe system on a time scale shorter than the lifetime of these excited states.

Since energy transfer to the exciting xenon metastable states is not energetically possible, we postulate that this transfer takes place by 3-body reaction (reaction 12) involving two xenon atoms and the excited mercury atoms. A lower limit is placed on this rate constant by the observed lifetime of the Xe_2^* radiation at low mercury pressure. This limit is 1.6×10^{-32} cm^6/sec.

Another piece of experimental evidence which tends to corroborate this picture is the fact that the observed lifetimes depend linearly on the Xe and Hg densities. If equilibrium were not established among the excited xenon states, then there should be a dependence of the observed lifetime of the 7^3S on the square of xenon pressure, since that would determine the formation rate of the Xe_2^*. This is not observed.

we will assume throughout that quenching of the excited states by collision with ground state xenon or mercury atoms is not an important process on the time scales observed. It is known that quenching of xenon excimers by ground state xenon and quenching of 6^3P mercury by ground state mercury is relatively slow [LEH73, HT71]. The postulate that ground state Xe atoms do not quench mercury 6^3P atoms is by analogy.

Hg 6^3P Metastable Levels and the Xe-Hg* Excimer

We are also proposing that collisional equilibrium is rapidly established between the 6^3P metastable levels of mercury and the mercury-xenon excimer. The 6^3P levels can be populated by one of three paths, radiation from $Hg(7^3S)$, collisional transfer from the Xe_2^* to the $Hg(6^3P)$ state (reaction 11), or collisional exchange (reaction 10), involving a ground state mercury atom exchanging with one of the xenon atoms in the Xe_2^*. Unless the well depth of the Xe-Hg metastable is very much larger than kT, collisional equilibrium between the atomic 6^3P levels and the Xe-Hg metastable will lead to most of the population residing in the 6^3P levels with only a small fraction in the Xe-Hg* state.

It is the 2700 Å excimer band radiation which is of primary interest for the Xe-Hg system. A rate equation for the state producing this emission can be written as

$$\frac{d}{dt} N = -(A_{16} f N) - (f N k_{19}[Hg])$$

where f is the fraction of total excited states in the excimer state at any given time; A is the radiative transition probability for the excimer state (reaction 16), N is the total number of excitations, and k_{19} is the rate coefficient as defined in Table II. This rate equation assumes that the principal loss mechanisms are by radiation out of the excimer state and by the formation of mercury excimers by reaction 19.

We assume that the $^3P_0$ metastable state of mercury, which should form a $^3O^-$ excimer with the xenon ground state, has a relatively low transition probability, since it is forbidden by symmetry as well as the spin-selection rule. Finally, we propose that the $^3P_0$ state is in collisional equilibrium with the $^3O^+$ state, which forms from the $^3P_1$ atomic level, and which radiates the 2700 Å band. The latter assumption is based on the observation that the deactivation of the $^3P_1$ to $^3P_0$ will probably be fairly rapid at these pressures, and that if the $^3P_0$ and its bound excimer $^3O^-$ level were not in collisional equilibrium with the $^3P_1$ and $^3O^+$ levels, we would expect the fluorescence yield from the 2700 Å band to be very small, which it is not.

When the fraction, f, of excited xenon mercury excimers is small ($\leq$ 10%), it can be given by an expression of the form

$$f \sim D[Xe]e^{-\Delta E/kT} ,$$

where ΔE is the effective well depth of the radiating state. The coefficient D gives the proportionality of f to the total pressure, which in this case will be taken to be the xenon pressure, and contains all the entropy dependent information. The radiative loss term can be determined by measuring the xenon dependence at low mercury pressures. If we plot the intercepts of the decay frequency versus mercury pressure with xenon as a parameter, we get the results shown in Figure 19. The slope of this line is 2.1×10^{-14} cm^3/sec. This rate constant is often called the collision-induced radiation rate, and by finding a value of f, the radiative lifetime of the excimer state can be deduced.

To find f, we need to obtain a measure of the effective well depth for our conditions. Since we have assumed collisional equilibrium between the $^3O^-$ and $^3O^+$ states, this determination should be made for the experimental conditions used, under the further assumption that the non-radiative loss of the excited states occurs only through reaction 19. We can get

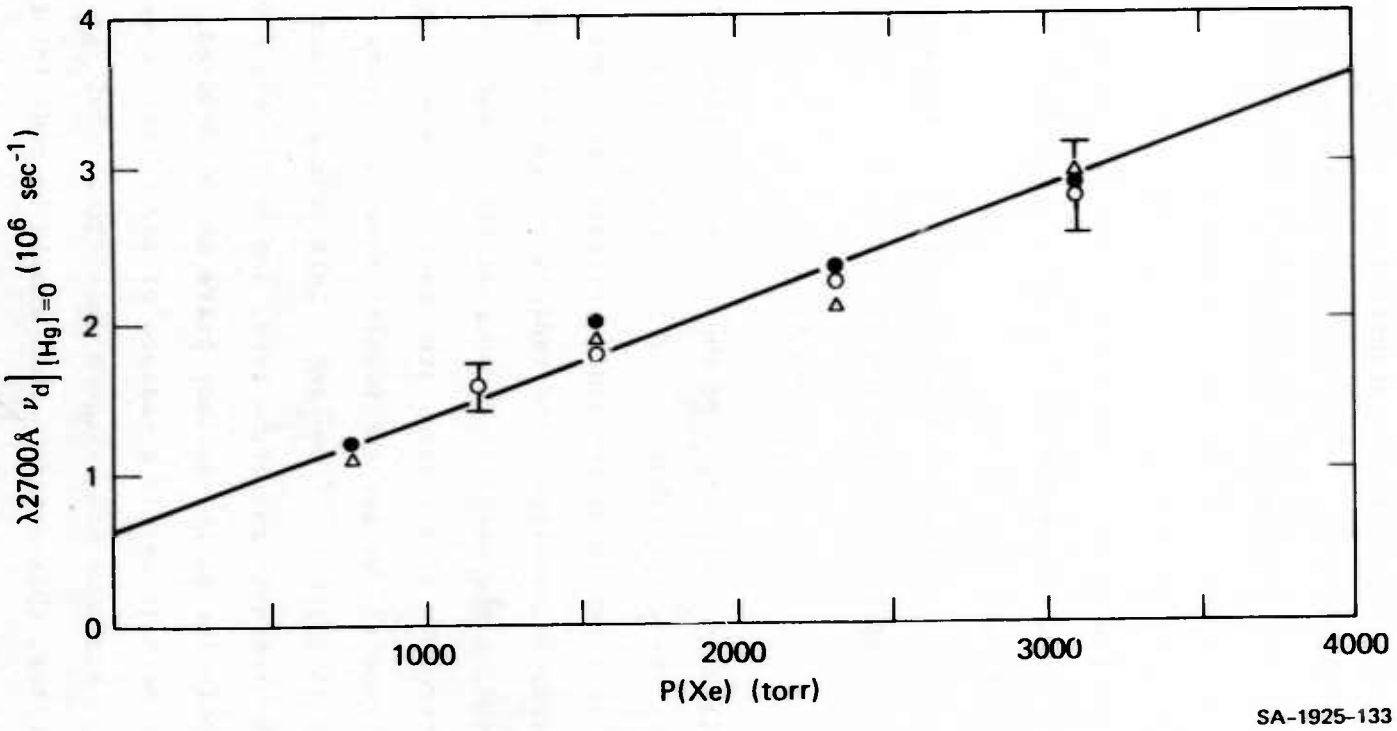

FIGURE 19 EXTRAPOLATED VALUE OF λ2700Å DECAY FREQUENCY AT [Hg]=0 VERSUS p(Xe)

The slope gives a rate coefficient of 2.1×10^{-14} cm^3/sec.

a measure of the well depth by plotting log ν_D/[Hg] versus 1/T for 45 psi Xe. This is done in Figure 20.

The ν_D values plotted were obtained in the following way. The data shown in Figure 14 were normalized to the same Xe pressure (60 psi) after the zero Xe pressure intercept had been subtracted. The normalized ν_D's obtained in this way are in substantial agreement. At each Hg density value (i.e., temperature) these normalized ν_D's were averaged and the plotted point is this average. The slope of this line gives ΔE of 1.3×10^3 cm^{-1}. This ΔE can be compared with determinations made by Strausz, et al. [SCP73], who were able to fit a Leonard Jones type potential to their low pressure line shape determinations, as well as the recent measurement of satellite bands in the xenon-mercury excimer by Kielkopf and Miller (KM74). The Strausz, et al., value is 1560 cm^{-1}, in reasonable agreement with ours, whereas Kielkopf and Miller derived a value of about 500 cm^{-1}, based on the vibrational spacing of very closely spaced lines observed adjacent to the 2537 atomic line. It seems likely that the KM value is for the more loosely bound $^3\Pi$ state, which will make transitions to a very flat part of the ground state curve.

These same data can be used to derive a measure of reaction 19. By plotting the normalized ν_D's against [Hg]$e^{\beta E/kT}$, Figure 21, we obtain a value of f $k_{19} = 3.1 \times 10^{-13}$ cm^3/sec. The [Hg] = 0 intercept is equal to k_{15} and agrees with our value derived from the data in Figure 19, within experimental error.

Fluorescence Yield and Efficiency

The fluorescence yield values shown in Table 1 and Figures 16 and 17 indicate the ratio of the observed number of photons emitted in the band relative to the number of photons observed from the Xe_2 excimer system without any mercury at all. It is easy to see from Figure 17b that the increased mercury pressure is very effective at quenching the Xe_2 excimer radiation, implying increased transfer into mercury excitation

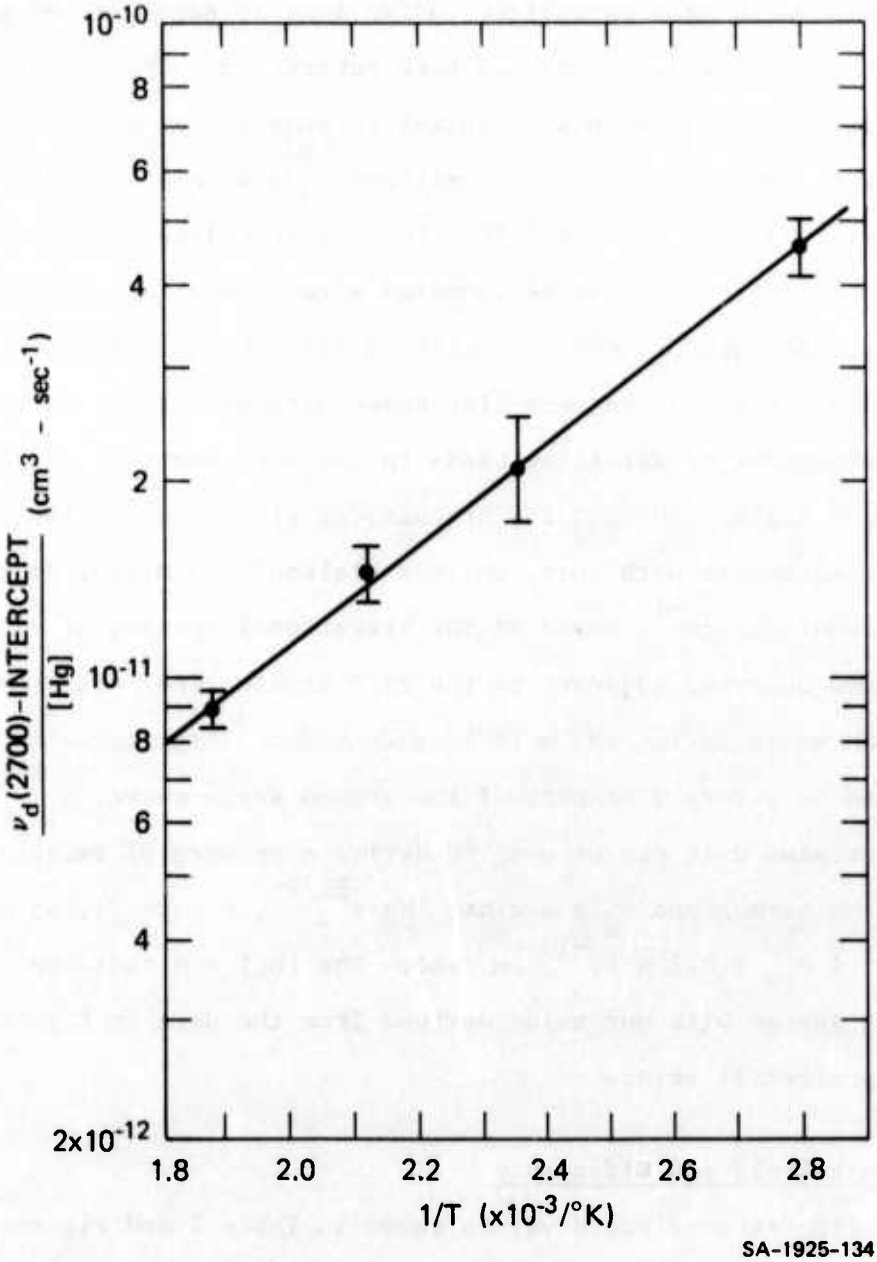

FIGURE 20 EFFECTIVE WELL DEPTH CALCULATION

The quantity subtracted from $\nu_d(2700)$ is the intercept value at zero xenon pressure. The slope yields 1300 cm^{-1}.

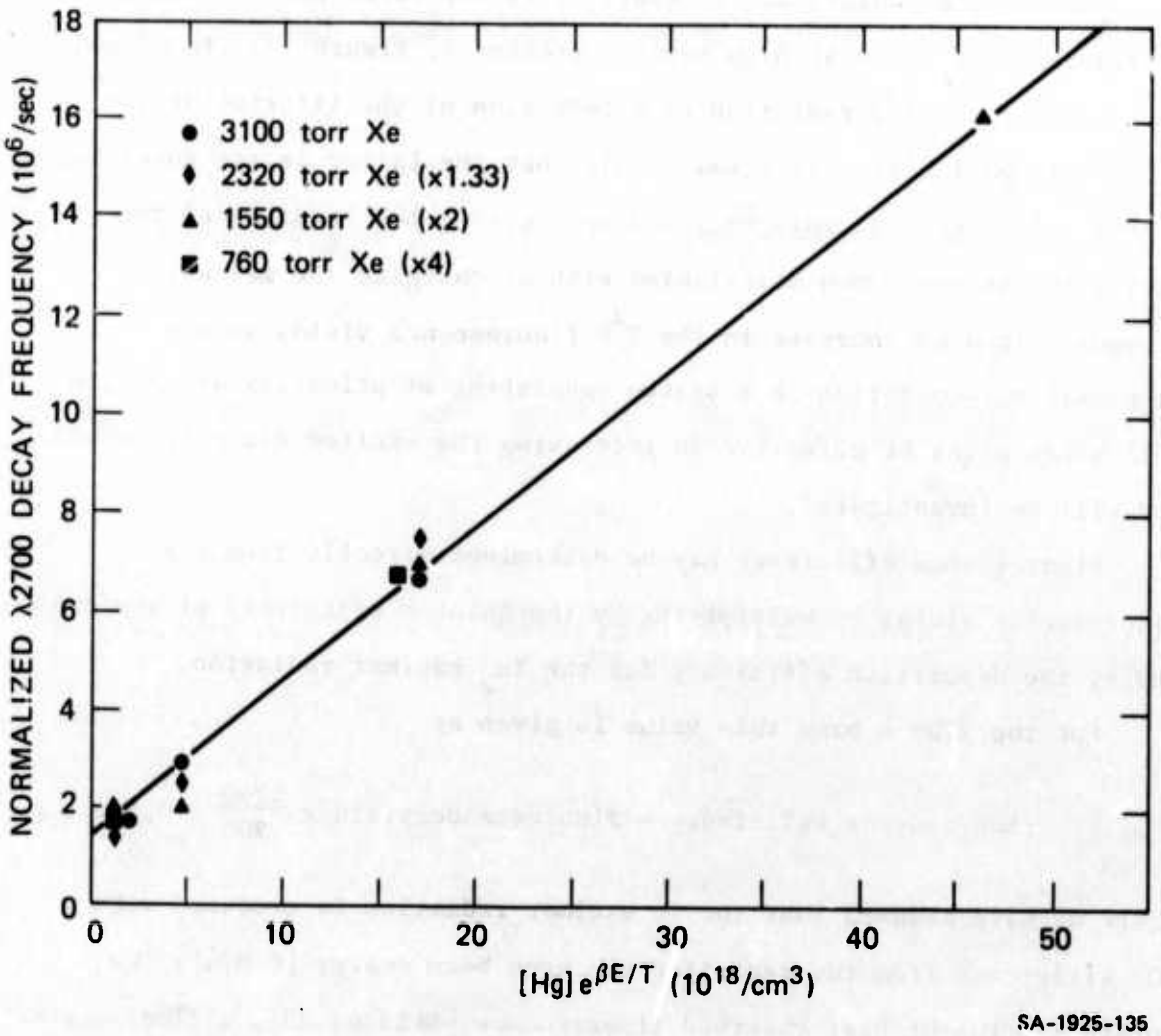

FIGURE 21 PLOT OF NORMALIZED λ2700Å DECAY FREQUENCY VERSUS TEMPERATURE COMPENSATED Hg DENSITY

The slope gives a measure of Hg_2^* excimer formation.

and the xenon-mercury excimer system. This, however, is balanced by the increased loss of the energy into the less useful Hg_2 excimer system, so that in the 2700 band system we notice that fluorescence yield has a maximum typically at 0.68×10^{17} Hg atoms/cm^3 while it is reduced at higher mercury pressures.

For the 7^3S radiations, however, it is not clear whether the reversal of fluorescence yield at high mercury pressures, Figure 17a, is caused by quenching of the 7^3S radiation or a reduction of the lifetime of the excited Xe particles. It seems likely that the latter is the governing factor. If a method could be found to increase the lifetime of the excitation in the xenon metastables without changing the mercury pressure, then an increase in the 7^3S fluorescence yields should be possible. Operation in a system consisting of primarily argon with .01% xenon might be effective in increasing the excited state lifetimes and will be investigated.

Fluorescence efficiency may be determined directly from the fluorescence yields by multiplying by the quantum efficienty of the photon and by the deposition efficiency for the Xe_2 excimer radiation.

For the 2700 Å band this value is given by

$$\text{fluorescence efficiency} = \text{fluorescence yield} \times \frac{1740}{2700} \times 0.3 \ ,$$

where we have assumed that the Xe excimer radiation is produced with a 30% efficiency from the deposited electron beam energy [CoM74]. We obtain for the highest observed fluorescence yield of 23%, a fluorescence efficiency of 4.4%.

The 2700 Å band output matches very well the excitation spectrum of CF_3I to produce the upper state of iodine atoms used in the iodine laser. For fluorescence efficiencies of 3 to 10%, the 2700 Å band could still be of significant interest for this use.

The peak 7^3S fluorescence efficiency is given by,

$$24\% \times \frac{1740}{4047} \times 0.3 = 3.0\% \quad .$$

This number is of considerable interest since the radiation intensity in this band is sufficient to suggest the possibility of laser action on this system.

It should be noted here that the fluorescence efficiency is a measure only of the efficiency with which photons emitted spontaneously are produced by these excited states. It does not measure efficiency with which the excited states themselves are produced because no determination of absolute densities can be made without a knowledge of quenching coefficients. This is mentioned because in an actual laser, if the stimulated emission occurs more rapidly than the spontaneous emission, higher overall efficiency becomes possible.

Peak Photon Flux and Gain

The peak photon fluxes given in Table III can be compared directly with the Ar/N_2 photon fluxes to give some measure of the gain to be expected on this particular transition, under the following assumptions. We will first assume that no absorption is produced by other species in the mixture or by the excited state. We will assume in addition that there is complete inversion of population, i.e., that the lower state is essentially unoccupied. This is certainly a good assumption for the 2700 Å band. Its validity in the case of the 7^3S system is unknown.

The ratio of the peak intensities gives a measure of the ratio of the gain, since the gain depends on the product of the stimulated emission coefficient and the number density, which is just a measure of the photon flux. If we restrict ourselves to the same wavelength bandwidth for each determination, then the gain ratios are valid within the above-mentioned assumptions. In addition, we should take into account the

Table III

PEAK PHOTON FLUXES[a]

P(Xe) torr	[Hg] atoms/cm^3	Temp °C	Xe_2^*	λ2100	λ2700	7^3S
760	7.5(15)	100	7 (19)	1 (18)	1.5(18)	5.2(19)
	3.7(17)	200	0.7	2.7	1.7	14
1130	7.5(15)	100	1.7	2.4	3	11
1550	7.5(15)	100	26	3.1	4	11
	3.7(17)	200	4	12	6.3	53
	1.5(18)	260	0.44	3	3	62
2320	7.5(15)	100	50	6.3	-	14
	6.8(16)	150	34	-	-	36
	3.7(17)	200	9.9	24	13	91
3100	7.5(15)	100	71	6.7	10	8.2
	6.8(16)	150	53	22	17	36
	3.7(17)	200	20	50	21	82

[a]In units of peak number of photons emitted/sec-cm^3 for a resolution of $\Delta\lambda$ = 3Å.

ratio of energy deposition for argon and xenon, which is 9.8/2.2 = 4.4 (p. 40). Comparison is then made by multiplying the peak of the 2+ system by this ratio. If we examine just the 1550 torr case, we see that the peak 2+ emission is 2.6×10^{20} photons/cm^3-sec x 4.4 = 1.1×10^{21} photons/cm^3-sec. The 7^3S at a density of $3.8 \times 10^{17}/cm^3$ is 5.3×10^{20} photons/cm^3-sec, suggesting that the gain ratio (N_2 2+)/(7^3S) = 1/2. For the 2700 Å system the peak emission intensity is 6.3×10^{18} photons/cm^3-sec, suggesting a gain ratio for (N_2 2+)/(2700 Å band) = 1/200.

E. Conclusions

The dynamic model which best fits our data is sketched in Figure 18. This shows that the xenon excimer and metastable are in equilibrium (produced by electrons), and that the xenon mercury excimer and the mercury metastables are in collisional equilibrium, probably brought about by atom collisions. The energy deposited in the rare gas exits through several channels: through the Xe_2^* excimer radiation, through the 2700 Å and 2100 Å xenon-mercury excimer bands, and through the mercury excimer radiation system, which radiates at 3300 and 4800 Å. Quenching of these excimer systems by the ground state atoms does not seem to be a serious loss.

Since both the xenon excimer and xenon mercury excimer radiations are linear in the total or rare gas pressure, we conclude that the fractional population of the excimer states in both cases is probably relatively small (i.e., 10% or less). An accurate determination of the equilibrium constant, particularly in the xenon-mercury case, will depend on more precise information about the well depth of the excimer state and the position of the potential minimum. However, we can say that the fractional population, coupled with the broad band of the xenon-mercury radiation, does not give great hopes for this being an efficient laser system because of the very high density of excited states required to reach threshold.

The maximum gain on the 2700 Å Xe-Hg band is 1/200 of the N_2 2+ system.

The 7^3S radiations which occur during collisions with ground state xenon atoms are much narrower and might lead to laser action if the absorption coefficient is sufficiently low. The estimate gain coefficient is 1/2 that of N_2 2+ system, assuming that absorption is negligible.

The fluorescent yield of the 2700 Å band is greater than 20%. This gives a maximum estimated efficiency of 4.4% for the emission of this radiation. Some increase in efficiency could result from using a mixture of argon and Xe as the rare gas energy donors.

The fluorescence yield for the 7^3S radiations can also be 10 to 20%. The potential for these bands as laser candidates with efficiencies of 5% or more should be investigated.

REFERENCES

ABO74 Ault, E.R., Bhaumik, M.L., Olson, N.T., J. Quantum Electron. QE-10, 624 (1974).

BB70 Bardsley, J.N., and Biondi, M.A., Advances in Atomic and Molecular Physics (Academic Press, New York, 1970), Chapter I.

BCL64 Barrat, J.P., Cojan, J.L., Lecluse, Y., C.R. Acad. Sci. Paris 260, 1893 (1965).

BDD74 Basov, N.G., Danilychev, V.A., Dolgikh, V.A., Kerimov, O.M., Donanov, A.N., and Suchkov, A.F., JETP Lett. 20, 53 (1974).

BMB65 Brewer, L., Meyer, B., and Brabson, G. D., J. Chem. Phys. 43, 3973 (1965).

BoM70 Boucique, R., and Mortier, P., J. Phys. D 3, 1905 (1970).

CoM74 Collier, F., and Michon, M., L'Onde Électrique 54, 467 (1974).

HGH74 Hill, R.M., Gutcheck, R.A., Huestis, D.L., Mukherjee, D., and Lorents, D.C., "Studies of E-Beam Pumped Molecular Lasers," Technical Report No. 3, SRI No. MP74-39, Contract N00014-72-C-0478, SRI Project 1925, Stanford Research Institute, Menlo Park, CA., July 1974.

HGH75 Huestis, D.L., Gutcheck, R.A., Hill, R.M., McCusker, M.V., Lorents, D.C., "Studies of E-Beam Pumped Molecular Lasers," Technical Report #4, ARPA Contract N00014-72-C-0478, Stanford Research Institute, Menlo Park, CA., January 1975.

HP74 Holt, R.A., and Pipkin, F.M., Phys. Rev. A, 9, 581 (1974).

HT71 Horiguchi, H., and Tsuchiya, S., Bull. Chem. Soc. Japan 44, 1213 (1971).

KFR74 This value is based on our analysis of the data presented in the paper.
Koehler, K.A., Ferderber, L.J., Redhead, R.L., and Ebert, R.J., Phys. Rev. A9, 768 (1974).

KM74 Kielkopf, J.T., and Miller, R.A., J. Chem. Phys. 61, 3304 (1974).

LEH73 Lorents, D.C., Eckstrom, D.J., and Huestis, D.L., "Excimer Formation and Decay Processes in Rare Gases," Final Report MP73-2, Contract N00014-72-C-0457, SRI Project 2018, Stanford Research Institute, Menlo Park, CA., September 1973.

LO72 Lorents, D.C., and Olson, R.E., "Excimer Formation and Decay Processes in Rare Gases," Semiannual Technical Report No. 1, Contract N00014-72-C-0457, SRI Project 2018, Stanford Research Institute, Menlo Park, CA, December 1972.

Ma65 Mahan, B., J. Chem. Phys. 43, 3080 (1965).

McD70 McDaniel, E.W., Ion Molecule Reactions (Wiley-Interscience, New York, 1970), p. 338.

MuZ71 Mumma, M.J. and Zipf, E.C., J. Opt. Soc. Am. 61, 83 (1971).

NMB73 Nelson, L.Y., Mullaney, G.J., and Byron, S.R., Appl. Phys. Lett. 22, 79 (1973).

Sam67 Samson, J.A.R., Techniques of Vacuum Ultraviolet Spectroscopy (John Wiley & Sons, Inc., New York, 1967), p. 212

SCP73 Strausz, O.P., Campbell, J.M., DePaoli, S., Sandhu, H.S., and Gunning, H.E., J. Am. Chem. Soc. 95, 732 (1973).

SDP72 Smith, D., Dean, A.G., and Plumb, I.C., J. Phys. B 5, 2134 (1972).

SeH74 Searles, S.K., and Hart, G.A., Appl. Phys. Lett. 25, 79 (1974).

SSJ63 Stair, R., Schneider, W.E., and Jackson, J.K., Appl. Optics 2, 1151 (1963).

TYF73 Tanaka, Y., Yoshino, K., and Freeman, D.E., J. Chem. Phys. 59, 5160 (1973).

WGH74 werner, C.W., George, E.V., Hoff, P.W., and Rhodes, C.K., Applied Physics Lett. 25, 235 (1974).

Wo75 Woodsworth, J., Sandia Laboratories, private communication.